Journal of Quantitative Spectroscopy & Radiative Transfer 208 (2018) 152–163

Contents lists available at ScienceDirect

Journal of Quantitative Spectroscopy & Radiative Transfer

journal homepage: www.elsevier.com/locate/jqsrt

Critical evaluation of measured rotational–vibrational transitions of four sulphur isotopologues of $S^{16}O_2$

Roland Tóbiás[a], Tibor Furtenbacher[a], Attila G. Császár[a,b,*], Olga V. Naumenko[c], Jonathan Tennyson[d], Jean-Marie Flaud[e], Praveen Kumar[f], Bill Poirier[a,f,*]

[a] MTA-ELTE Complex Chemical Systems Research Group, Pázmány Péter sétány 1/A, Budapest H-1117, Hungary
[b] Institute of Chemistry, Eötvös Loránd University, 112, P.O. Box 32, Budapest H-1518, Hungary
[c] Institute of Atmospheric Optics, Russian Academy of Sciences, Tomsk, Russia
[d] Department of Physics and Astronomy, University College London, WC1E 6BT, London, United Kingdom
[e] Laboratoire Interuniversitaire des Systemes Atmosphériques (LISA), UMR CNRS 7583, Universités Paris Est Créteil et Paris Diderot, Institut Pierre Simon Laplace, 61 Avenue du Général de Gaulle, 94010 Créteil Cedex, France
[f] Department of Chemistry and Biochemistry, Texas Tech University, Lubbock, Texas, 79409-1061, USA

ARTICLE INFO

Article history:
Received 19 July 2017
Revised 4 January 2018
Accepted 5 January 2018
Available online 6 January 2018

Keywords:
SO_2
Experimental rovibrational transitions
Atmospheric physics
Energy levels
Spectrocopic networks
MARVEL
Spectroscopic bridges
Information system
Infrared and microwave spectra
Effective Hamiltonian models

ABSTRACT

A critical evaluation and validation of the complete set of previously published experimental rotational–vibrational line positions is reported for the four stable sulphur isotopologues of the semirigid SO_2 molecule – *i.e.*, $^{32}S^{16}O_2$, $^{33}S^{16}O_2$, $^{34}S^{16}O_2$, and $^{36}S^{16}O_2$. The experimentally measured, assigned, and labeled transitions are collated from 43 sources. The $^{32}S^{16}O_2$, $^{33}S^{16}O_2$, $^{34}S^{16}O_2$, and $^{36}S^{16}O_2$ datasets contain 40,269, 15,628, 31,080, and 31 lines, respectively. Of the datasets collated, only the extremely limited $^{36}S^{16}O_2$ dataset is not subjected to a detailed analysis. As part of a detailed analysis of the experimental spectroscopic networks corresponding to the ground electronic states of the $^{32}S^{16}O_2$, $^{33}S^{16}O_2$, and $^{34}S^{16}O_2$ isotopologues, the MARVEL (Measured Active Rotational–Vibrational Energy Levels) procedure is used to determine the rovibrational energy levels. The rovibrational levels and their vibrational parent and asymmetric-top quantum numbers are compared to ones obtained from accurate variational nuclear-motion computations as well as to results of carefully designed effective Hamiltonian models. The rovibrational energy levels of the three isotopologues having the same labels are also compared against each other to ensure self-consistency. This careful, multifaceted analysis gives rise to 15,130, 5852, and 10,893 validated rovibrational energy levels, with a typical accuracy of a few 0.0001 cm^{-1}, for $^{32}S^{16}O_2$, $^{33}S^{16}O_2$, and $^{34}S^{16}O_2$, respectively. The extensive list of validated experimental lines and empirical (MARVEL) energy levels of the $S^{16}O_2$ isotopologues studied are deposited in the Supplementary Material of this article, as well as in the distributed information system ReSpecTh (http://respecth.hu).

1. Introduction

The spectroscopy of the SO_2 molecule – though never out of fashion – has witnessed an explosive resurgence of interest in the past few years. By now, there is an extensive literature on the spectroscopy of SO_2, both in its ground $\tilde{X}^1A_1$ electronic state [1–63], and involving the electronically excited states, particularly $\tilde{C}^1B_2$ [64–96]. As a key player in the acid rain saga, SO_2 in the atmosphere has been studied for some decades. However, two comparatively new – and rather different – SO_2 applications have emerged more recently, resulting in a great demand for accurate, high resolution, and isotope-specific spectroscopic data.

The first application is of astrophysical origin. SO_2 has been observed in the interstellar medium, and is of great interest for extrasolar planetary atmospheres [97–102]. While not the most prevalent compound in these environments, the SO_2 rovibrational spectroscopic signal can drown out those of other molecular species of interest. To address this situation, the community has recognized the need for high-resolution rovibrational spectra of SO_2 on the ground $\tilde{X}^1A_1$ electronic state, which can be used to "weed out" the SO_2 background signal, thereby revealing the "flowers" of interest [50,51,58]. In this astrophysical context, the two most prevalent sulphur isotopologues – *i.e.*, $^{32}S^{16}O_2$ and $^{34}S^{16}O_2$, which together account for over 99% of all $S^{16}O_2$ under regular circumstances – are by far the most important.

* Corresponding authors.
E-mail addresses: csaszar@chem.elte.hu (A.G. Császár), bill.poirier@ttu.edu (B. Poirier).

https://doi.org/10.1016/j.jqsrt.2018.01.006
0022-4073/

On the other hand, *all four* stable sulphur isotopologues of $S^{16}O_2$ – *i.e.*, $^{32}S^{16}O_2$, $^{33}S^{16}O_2$, $^{34}S^{16}O_2$, and $^{36}S^{16}O_2$ – are vitally important for the second application, which is astrobiological and paleogeological in nature. Specifically, it pertains to the "oxygen revolution" that led to respiring life forms on our planet, circa 2.5 billion years ago. This seminal event was coincident with a sudden and dramatic disappearance of the "S-MIF" (sulphur mass-independent fractionation) signal observed in the Archean rock record [103–109] – which can therefore serve as a proxy for Archean atmospheric oxygen levels, provided that the specific mechanism that gave rise to the S-MIF can be properly identified and characterized.

In general terms, S-MIF is thought to arise from SO_2 photodissociation in the atmosphere, following $\tilde{C}^1B_2 \leftarrow \tilde{X}^1A_1$ ultraviolet photoabsorption [108], although the specific mechanism still remains unknown [53,54,68,72,74–76,81–86,88–90,92–96]. Among those mechanisms that have been proposed, some, such as "self-shielding" [54,81,83,85,88,94,95], depend intimately on the precise placement of rovibrational energy levels, whose isotope shifts vary by a few cm^{-1} for the different isotopologues (*vide infra*). Validation therefore requires high-resolution spectra for all sulphur isotopologues of $S^{16}O_2$ – with at least three distinct sulphur isotopes needed to even define S-MIF, and all four necessary to reproduce/identify the key S-MIF trends observed in the rock record. However, up to 2017, with respective abundances of only 0.007 486 5 and 0.000 145 9, the ^{33}S and ^{36}S isotopologues have been neglected in most experimental work – with those few experiments that have been performed generally characterized by far fewer – and/or lower resolution – spectral lines. In 2017, Flaud (one of the present authors) and his co-workers published two high-resolution experimental spectroscopic studies [62,63] on $^{33}S^{16}O_2$; both have been utilized during the present analysis.

In principle, theoretical and computational modeling can help to validate and extend the experimentally available spectroscopic information. Computational modeling requires detailed potential energy surfaces (PES), as well as (transition) dipole moment surfaces (DMS), and it is capable of achieving sub-cm^{-1} accuracies [110]. Several such highly-accurate surfaces have emerged in recent years for SO_2 [33,50,51,58,80,84,86,90,111]. One of the present authors (Poirier), together with Alexander, Guo, and co-workers, was involved in the development of new purely *ab initio* surfaces for the $\tilde{X}^1A_1$ and $\tilde{C}^1B_2$ electronic states of SO_2, using the explicitly correlated F12 technique of electronic structure theory [90]. Accurate rovibrational state computations are being performed on these surfaces for all four sulphur isotopologues. In the $\tilde{X}^1A_1$ case, comparison [53,54] of these purely *ab initio* computations with previous results using the older semiempirical PES of Kauppi and Halonen [23], and with experiment, is highly encouraging – achieving agreement on the order of 1 cm^{-1}. In the $\tilde{C}^1B_2$ case, the purely *ab initio* vibrational state computations [94] have already helped to resolve several spectral assignment controversies [66,67,74,77,79,83] – corroborating previous work of Field and co-workers [89,91–93]. Moreover, together with the DMS, a purely *ab initio* simulation of the experimental photoabsorption spectrum has also recently been performed, which has proven to be remarkably accurate, both in terms of intensities and peak placements [95].

Following a different tack, Schwenke and co-workers [51,58] have developed an empirically-corrected PES for $\tilde{X}^1A_1$, designed to reproduce a large number of HITRAN [112] rovibrational levels of the $^{32}S^{16}O_2$ isotopologue and make predictions for missing $^{32}S^{16}O_2$ bands and those of other species, such as $^{34}S^{16}O_2$, $^{33}S^{16}O_2$, $^{32}S^{16}O^{18}O$, and $^{32}S^{18}O_2$. With help from one of the present authors (Tennyson), a S–O stretch basis defect was identified and fixed [58], giving rise to a more robust and accurate PES [51], refined using $^{32}S^{16}O_2$ data. The fixed PES has been adopted to perform accurate rovibrational computations for all four $S^{16}O_2$ isotopologues, yielding transitions in agreement with their experimental counterparts to within 0.03 cm^{-1}. To date, these are the most accurate and comprehensive $\tilde{X}^1A_1$ rovibrational computations for SO_2.

Quantum chemical computation of rovibrational states is highly useful, providing levels to compare with putative experimental data. Nevertheless, variational nuclear motion computations fail to provide unambiguous v and J_{K_a,K_c} quantum number labels, where $v = (v_1v_2v_3)$ and J_{K_a,K_c} correspond to the vibrational parent (normal-mode) and asymmetric-top notation [113], respectively. Of these quantum numbers only J, the quantum number of overall rotation, is a good quantum number. For large J values even at relatively low energy, the rovibrational spectrum for SO_2 becomes very dense – introducing potential level/label challenges (especially when K_a approaches J). This is the case even though the molecule in its $\tilde{X}^1A_1$ electronic state is rather rigid, which would suggest that "approximate" labels should be assignable.

In any event, there is a demand for accurate, reliable methods for assigning and validating levels and labels to experimental (and in the label case, theoretical) spectroscopic data. In this paper, we adopt a combined approach, wherein the MARVEL (Measured Active Rotational–Vibrational Energy Levels) procedure [114] is used (within the frame of a detailed spectroscopic network [114–120] analysis) for obtaining accurate empirical (hereafter called MARVEL) energy levels, and effective Hamiltonian (EH) methods (conventional EH models and a J-dependent rotational Hamiltonian approach) are used for the validation of the rovibrational assignments. Specifically, we first apply the useful tools of the theory of spectroscopic networks to all of the experimentally available rovibrational transitions on the ground $\tilde{X}^1A_1$ electronic state, for the three most common sulphur isotopologues of $S^{16}O_2$. From the cleansed database, a comprehensive list of MARVEL energy levels emerges for $^{32}S^{16}O_2$, $^{33}S^{16}O_2$, and $^{34}S^{16}O_2$, together with an assessment of uncertainty for each level. The $(v_1v_2v_3)J_{K_a,K_c}$ assignments coming from the literature are carefully checked against their counterparts determined by effective Hamiltonian models.

The theory of spectroscopic networks is well established, and amply discussed in the literature [117,119]; nevertheless, a brief summary, with a new feature related to graph bridges [120,121] is presented in Section 2.1. Following the description of the spectroscopic network analysis, the EH methods employed are outlined in Section 2.2 (a detailed exposition on the J-dependent rotational Hamiltonian procedure is postponed for future work).

The combination of the spectroscopic network analysis and the EH approaches may be applied to any molecular system, in principle providing reliable levels and labels for any collection of experimental rovibrational data. In practice, the availability of too few observed and assigned spectral lines may limit the applicability of the spectroscopic network analysis, as found to be the case here for $^{36}S^{16}O_2$ (see Section 3). Likewise, extremely floppy systems, for which resonance interactions are very pronounced, may give rise to issues related to the use of EH models. Nevertheless, this is not the case for the experimentally available spectroscopic information for the $S^{16}O_2$ isotopologues.

2. Methodology

2.1. Spectroscopic network analysis

In order to provide the best estimates for the rovibrational energy levels of three of the four $S^{16}O_2$ isotopologues investigated, all of the observed high-resolution rovibrational lines, as collated from the literature, were analyzed simultaneously by constructing a *spectroscopic network* (SN) [115,117] for each isotopologue. SNs offer a useful framework to validate, revise, and correct transitions in

the complete database of measured spectroscopic transitions. In a SN, the vertices correspond to energy levels, and the connecting edges to measured lines (transitions).

For symmetry and other reasons, it can happen that an experimental SN consists of multiple *components* [117] – *i.e.*, collections of energy levels that are unconnected by any measured transitions. The components which contain the lowest energy levels of the distinct nuclear-spin isomers of a molecule are called the *principal components* (PC). As the ^{16}O nucleus has zero spin, the rovibrational transitions of each $S^{16}O_2$ isotopologue should form a single PC, at least in principle. In practice, an experimental SN may include other components, referred to as *floating components* (FCs) [117]. These FCs are not of direct use to assess the energy-level structure of a molecule, unless additional transitions are subsequently measured that link the FC levels to those of the PC.

A *cycle* is a closed loop of transitions. Due to the large number of cycles in measured SNs, the compatibility of line positions and their uncertainties can be examined by using the *law of energy conservation* (LEC) [120]. If a transition in a cycle is measured inaccurately, assigned improperly, or its assigned uncertainty is lower than it should be, then the discrepancy of the given cycle, defined as the absolute signed sum of the transition wavenumbers, becomes higher than the experimental tolerance threshold, indicating a conflict among the lines in the cycle considered [120]. For this purpose, the ECART (Energy Conservation Analysis of Rovibronic Transitions) code was applied to determine and characterize *minimum cycle bases* (MCBs) of the SNs of the three $S^{16}O_2$ isotopologues under study (see 17ToFuCs [120] for details).

For a SN that includes no *outliers* (incorrect or incorrectly labeled transitions), empirical energy levels can be deduced using the MARVEL procedure [114–118]. During a MARVEL analysis of the experimentally observed transitions, the following objective function is minimized:

$$S(\mathbf{E}) = \sum_{i=1}^{N_T} \frac{1}{\delta_i^2} \left(\sigma_i - E_{\mathrm{up}(i)} + E_{\mathrm{low}(i)}\right)^2, \tag{1}$$

where (a) $\mathbf{E} = \{E_1, E_2, ..., E_{N_L}\}^T$ is the column vector of N_L (unknown) energy values with the transpose operation T, (b) σ_i is the experimental wavenumber of the ith transition with δ_i uncertainty, (c) N_T is the number of transitions observed, and (d) up(i) and low(i) are the indices of the upper and lower levels corresponding to the ith transition, respectively.

It is obvious that there exists a unique $\bar{\mathbf{E}} = \{\bar{E}_1, \bar{E}_2, ..., \bar{E}_{N_L}\}^T$ minimum for the function $S(\mathbf{E})$, whose $\bar{E}_j$ component is called the jth *empirical (MARVEL) energy level* in the SN. The uncertainty of the level $\bar{E}_j$, designated by ϵ_j, is approximated as

$$\epsilon_j = \sqrt{1 / \sum_{i=1}^{N_T} \left(I_{\mathrm{up}(i)j} + I_{\mathrm{low}(i)j}\right) \delta_i^{-2}}, \tag{2}$$

where I_{kl} is the (k, l)-entry of the identity matrix I of size $N_L \times N_L$.

Unfortunately, individual uncertainties are usually not reported in the data sources; thus, we are forced to use reasonable uncertainty estimates based on the experimental information available. However, each approximate δ_i uncertainty should be *consistent* with the $\Delta_i = \sigma_i - \bar{E}_{\mathrm{up}(i)} + \bar{E}_{\mathrm{low}(i)}$ residual, *i.e.*, satisfy the relation $\delta_i \geq |\Delta_i|$. To ensure the consistency of the uncertainties, we apply an iterative procedure, similar to *robust weighting* [122], during which δ_i is increased to $1.1|\Delta_i|$ whenever $\delta_i < |\Delta_i|$, and the MARVEL analysis is repeated until all uncertainties become consistent with the corresponding residuals. For all three $S^{16}O_2$ isotopologues these "adjusted" uncertainties were used to obtain the MARVEL energy levels.

In addition to FCs, *spectroscopic bridges* (SB) [121], defined as transitions whose deletion increases the number of components in a given SN, introduce difficulties for both the ECART and MARVEL algorithms. SBs therefore require special attention. In particular, if the transition wavenumber of a SB is incorrect or inaccurate, then the energies of the rovibrational states connected by this bridge to a PC will be shifted. By removing all SBs, the *maximum bridgeless subnetwork* (MBS) of the SN is obtained, whose components are called *bridge components* (BC) [121]. By means of the MBS, the *resistance* of energy levels, reflecting our trust in the accuracy of the levels, can be characterized as follows. An energy level is: (a) *protected*, if it belongs to the same bridge component as the lowest energy level of the corresponding PC; (b) *semiprotected*, if it lies in a different BC that also includes other levels; and (c) *unprotected*, if it lies all alone in its own BC with no other levels. If a bridge connects two BCs of several levels, it is called an *internal bridge*. Furthermore, if a bridge is incident to an unprotected level, it is an *external bridge*. This classification of MARVEL energy levels was built into the latest version of the MARVEL code.

2.2. Effective Hamiltonian (EH) models

2.2.1. Conventional EH method

The rovibrational energy levels of the $S^{16}O_2$ isotopologues can be characterized with the following rovibrational Hamiltonian operator [48]:

$$\hat{H} = \sum_{v,v'} |v\rangle \langle v'| \hat{H}^{vv'}, \tag{3}$$

where $|v\rangle$ is the vibrational eigenfunction of the state v, the diagonal $\hat{H}^{vv}$ operator describes the unperturbed rotational structures of the vibrational state v, and the off-diagonal $\hat{H}^{vv'}$ term ($v \neq v'$) represents the resonance interaction between states v and v'.

In the present study, the following 12th-degree diagonal Hamiltonian has been used, based on A-reduction and the I^r representation [123–126]:

$$\begin{aligned}
\hat{H}^{vv} = {} & E^v + \left(A^v - \frac{1}{2}\left(B^v + C^v\right)\right)\hat{J}_z^2 + \frac{1}{2}\left(B^v + C^v\right)\hat{J}^2 + \frac{1}{2}\left(B^v - C^v\right)\hat{J}_{xy}^2 \\
& - \Delta_K^v \hat{J}_z^4 - \Delta_{JK}^v \hat{J}_z^2 \hat{J}^2 - \Delta_J^v \hat{J}^4 - \delta_K^v \left\{\hat{J}_z^2, \hat{J}_{xy}^2\right\} - 2\delta_J^v \hat{J}^2 \hat{J}_{xy}^2 + H_K^v \hat{J}_z^6 \\
& + H_{KJ}^v \hat{J}_z^4 \hat{J}^2 + H_{JK}^v \hat{J}_z^2 \hat{J}^4 + H_J^v \hat{J}^6 + \left\{h_K^v \hat{J}_z^4 + h_{JK}^v \hat{J}_z^2 \hat{J}^2 + h_J^v \hat{J}^4, \hat{J}_{xy}^2\right\} + L_K^v \hat{J}_z^8 \\
& + L_{KKJ}^v \hat{J}_z^6 \hat{J}^2 + L_{JK}^v \hat{J}_z^4 \hat{J}^4 + L_{JJK}^v \hat{J}_z^2 \hat{J}^6 + L_J^v \hat{J}^8 \\
& + \left\{l_K^v \hat{J}_z^6 + l_{KJ}^v \hat{J}_z^4 \hat{J}^2 + l_{JK}^v \hat{J}_z^2 \hat{J}^4 + l_J^v \hat{J}^6, \hat{J}_{xy}^2\right\} + P_K^v \hat{J}_z^{10} + P_{KKJ}^v \hat{J}_z^8 \hat{J}^2 \\
& + P_{KJ}^v \hat{J}_z^6 \hat{J}^4 + P_{JK}^v \hat{J}_z^4 \hat{J}^6 + P_{JJK}^v \hat{J}_z^2 \hat{J}^8 + P_J^v \hat{J}^{10} \\
& + \left\{p_K^v \hat{J}_z^8 + p_{KKJ}^v \hat{J}_z^6 \hat{J}^2 + p_{JK}^v \hat{J}_z^4 \hat{J}^4 + p_{JJK}^v \hat{J}_z^2 \hat{J}^6 + p_J^v \hat{J}^8, \hat{J}_{xy}^2\right\} \\
& + S_K \hat{J}_z^{12} + S_{KKJ} \hat{J}_z^{10} \hat{J}^2 + S_{KKJ} \hat{J}_z^8 \hat{J}^4 + S_{KJ} \hat{J}_z^6 \hat{J}^6 + S_{JK} \hat{J}_z^4 \hat{J}^8 \\
& + S_{JJK} \hat{J}_z^2 \hat{J}^{10} + S_J \hat{J}^{12},
\end{aligned} \tag{4}$$

where $\hat{J}_x$, $\hat{J}_y$, and $\hat{J}_z$ are the three components of the rotational angular momentum operator $\hat{J}$, (x, y, z) is a permutation of the principal axes (a, b, c), and the curly brackets denote the anticommutator.

The Fermi interaction of two vibrational states v and v' of the same symmetry has been taken into account as [127]

$$\begin{aligned}
{}^F\hat{H}^{vv'} = {} & {}^{vv'}F_0 + {}^{vv'}F_K \hat{J}_z^2 + {}^{vv'}F_J \hat{J}^2 + {}^{vv'}F_{Kxy} \hat{J}_{xy}^2 + {}^{vv'}F_{Kxy} \left\{\hat{J}_z^2, \hat{J}_{xy}^2\right\} \\
& + 2\,{}^{vv'}F_{Jxy} \hat{J}^2 \hat{J}_{xy}^2.
\end{aligned} \tag{5}$$

The Coriolis interaction of vibrational states of different symmetry was included *via* the following interaction term [127]:

$$
\begin{aligned}
{}^{\mathrm{C}}\hat{H}^{vv'} = {}& {}^{vv'}C_{yKK}\left\{i\hat{J}_y,\hat{J}_z^4\right\} + {}^{vv'}C_{yJ}i\hat{J}_y\hat{J}^2 + {}^{vv'}C_{xzK}\left\{\hat{J}_x,\hat{J}_z^3\right\} \\
& + {}^{vv'}C_{yK}\left\{i\hat{J}_y,\hat{J}_z^2\right\} + {}^{vv'}C_{y}i\hat{J}_y + {}^{vv'}C_{xz}\left\{\hat{J}_x,\hat{J}_z\right\} + {}^{vv'}C_{xzJ}\left\{\hat{J}_x,\hat{J}_z\right\}\hat{J}^2 \\
& + {}^{vv'}C_{xzKJ}\left\{\hat{J}_x,\hat{J}_z^3\right\}\hat{J}^2 + {}^{vv'}C_{xzJJ}\left\{\hat{J}_x,\hat{J}_z\right\}\hat{J}^4.
\end{aligned} \tag{6}
$$

For semirigid molecules, like SO_2, the conventional EH models should work well. Thus, the literature was searched for conventional EH parameters for the various vibrational states of $^{32}S^{16}O_2$, $^{33}S^{16}O_2$, and $^{34}S^{16}O_2$. These rovibrational parameters [11,36,39,42,44,45,48,52,55–57,62,63,128,129], complying with the equations given above, formed the basis of our own fits to the MARVEL energy levels for the three isotopologues. These conventional EH models with the optimized parameters have been used to generate energy levels as well as rovibrational labels to be compared with the MARVEL energies and labels of this study.

2.2.2. J-dependent rotational Hamiltonian approach

If the resonance interactions are neglected in Eq. (3), the diagonal $\hat{H}^{vv}$ operators can be treated separately and split as

$$\hat{H}^{vv} = \hat{H}_v + \hat{H}_{\mathrm{R}}, \tag{7}$$

where $\hat{H}_v$ and $\hat{H}_{\mathrm{R}}$ are the pure vibrational and pure asymmetric-rotor Hamiltonians, respectively.

A further simplification ensues in the conventional EH formalism if one fits the J blocks independently. At the level of individual J blocks, then – with $\sim$ denoting the matrix block for a given J – we have the following useful relation:

$$\tilde{J}_x^2 + \tilde{J}_y^2 + \tilde{J}_z^2 = \hbar^2 J(J+1)\tilde{I}, \tag{8}$$

where $\tilde{I}$ is the matrix representation of the identity operator.

From Eq. (8), together with other arguments [123–126], it can be shown that $\hat{H}_{\mathrm{R}}$ may be *uniquely* expanded in the form

$$\tilde{H}_{\mathrm{R}}^{J} = 2\pi\hbar c\left\{C_{(0,0)}^{J}J(J+1)\tilde{I} + \sum_{(m,n)\neq(0,0)} C_{(m,n)}^{J}\left[\frac{\tilde{J}_{\Delta}^{m}\tilde{J}_z^{n} + \tilde{J}_z^{n}\tilde{J}_{\Delta}^{m}}{2\hbar^{m+n}}\right]\right\}, \tag{9}$$

where $\tilde{J}_{\Delta}^2 = (\tilde{J}_y^2 - \tilde{J}_x^2)/2$, and m and n are both even nonnegative integers. We again stress that Eq. (9) applies at the *block* level only, for a given J value.

From the $C_{(m,n)}^{J}$ parameters, the conventional (prolate) rotational constants $C < B < A$ for the x, y, and z axes, respectively, can also be obtained:

$$
\begin{aligned}
C &= C_{(0,0)}^{J} - C_{(2,0)}^{J}/2 \\
B &= C_{(0,0)}^{J} + C_{(2,0)}^{J}/2 \\
A &= C_{(0,0)}^{J} + C_{(0,2)}^{J}.
\end{aligned}
$$

For an almost prolate rotor such as SO_2, with $z = a$, it is generally more effective to expand further in n than in m. In Section 5.2, for example, we consider a simple six-parameter model, including just the terms $(m,n) = (0,0), (2,0), (0,2), (0,4), (0,6), (0,8)$. In comparison with the conventional EH expansion, there are significantly fewer terms (*i.e.*, fitting parameters) up to a given order $(m+n)$. Moreover, root-mean-square deviations (RMSD) for the optimally-fitted eigenvalues of $\hat{H}^{vv}$ in Eq. (7) to a reference energy level dataset – if conducted up to the same order – will be *smaller* in the J-dependent case, because each fit is applied to a smaller dataset.

In practice, the optimal $C_{(m,n)}^{J}$ values themselves do not change much with J, except for the smallest J or largest $(m+n)$ values. Indeed, the J dependence of the $C_{(m,n)}^{J}$, as well as the RMSDs, is usually smooth and monotonic. This can be exploited to analyze spectroscopic labels for individual rovibrational levels.

3. Experimental data sources

For $^{32}S^{16}O_2$, $^{33}S^{16}O_2$, and $^{34}S^{16}O_2$, there exists a considerable number of at least partially assigned experimental spectra, recorded in absorption at microwave and infrared wavelengths [1,3–15,17,18,21,22,24,25,27,28,32,34,36–39,42–46,48,49,52,55–57,62,63,99,102]. The studies indicated represent an extensive knowledge about rotations and vibrations on the ground electronic state of the three $S^{16}O_2$ isotopologues. Note that the sources 72HiCaKeCl [7], 73CoFoTea [8], 73CoFoTeb [9], and 75BaSeJoDu [10] have been neglected in our final spectroscopic network analysis because the transitions reported there seemingly suffer from significant uncertainty. Almost all of these transitions have been measured later, and a simple recalibration, similar to the one performed in Ref. [130] and for 93LaPiFlCa [25], 10TaChStGi [43], 16UlBeGrBua [55], 16UlBeGrBub [57], and 17CeTaPuCh [102] during this study, did not help to improve accuracy.

As to $^{36}S^{16}O_2$, only some microwave measurements can be found in the literature [13]; thus, further high-resolution studies would be needed to justify an investigation based on the theory of spectroscopic networks. In the remainder of this paper, the data corresponding to the $^{32}S^{16}O_2$, $^{33}S^{16}O_2$, and $^{34}S^{16}O_2$ isotopologues are discussed.

There are numerous studies [30,31,50,51,53,54,58,77] that provide computed rovibrational energy levels for the $\tilde{X}^1A_1$ state of $S^{16}O_2$. Mixed experimental and theoretical lines are accessible in the GEISA [131] and HITRAN [112,132] databases, as well.

Table 1 contains information on the transitions reported in the data sources identified in the literature. The tags applied in this study for these data sources are also given in Table 1. As shown by the column 'A/V', a comparatively small number of non-validated lines (in fact, 83) are present in the $^{32}S^{16}O_2$, $^{33}S^{16}O_2$, and $^{34}S^{16}O_2$ datasets – which indicates an essentially perfect agreement among the experimental data coming from many different sources. To confirm the compatibility of the measurements, the *averages of positive absolute residuals* (APAR) and the *largest absolute residuals* (LAR) are also listed in Table 1. For the jth source, APAR and LAR are defined as

$$\mathrm{APAR}_j = \frac{1}{n_j}\sum_{i=1}^{n} b_{ij}|\Delta_i| \tag{10}$$

and

$$\mathrm{LAR}_j = \max_{i=1}^{n} b_{ij}|\Delta_i|, \tag{11}$$

where n is the number of (validated) lines in the SN of the given species, n_j is the number of lines with nonzero residual, and b_{ij} is a binary parameter ($b_{ij} = 1$ if the ith transition originates from the jth source, otherwise $b_{ij} = 0$).

4. Data treatment

The collated experimental data, see Table 1, were subject to a thorough cleansing. In the first step, transcription errors and formatting problems were corrected in the experimental linelist. Then, a test was executed on the lines to check whether the proper selection rules are satisfied. In the case of $S^{16}O_2$ isotopologues, each $(\nu_1\nu_2\nu_3)J_{K_a,K_c}$ label must obey, due to the Pauli principle, the following two rules:

$$(-1)^{\nu_3+K_a+K_c} = 1 \tag{12}$$

and

$$K_a + K_c \in \{J, J+1\}. \tag{13}$$

Since only dipole-allowed transitions are present in the dataset, each line $(\nu'_1\nu'_2\nu'_3)J'_{K_{a'},K_{c'}} \leftarrow (\nu''_1\nu''_2\nu''_3)J''_{K_{a''},K_{c''}}$ must also re-

Table 1
Data sources and their characteristics for the $S^{16}O_2$ isotopologues considered.[a]

Species	Tag	Range/cm^{-1}	A/V	APAR/10^{-9} cm^{-1}	LAR/10^{-9} cm^{-1}
$^{32}S^{16}O_2$	78Lovas [13]	0.017393–12.001	1557/1557	5752	421,125
	98BeTrKoKl [28]	0.23915–34.367	78/78	1774	23,115
	64MoKiSaHi [5]	0.26976–1.8681	**83/82**	19,008	250,163
	79BeDrMa [14]	0.39323–0.48659	3/3	2200	3242
	69Saito [6]	0.42653–2.3605	52/52	301	8174
	64BaBe [4]	0.53532–2.3607	86/86	2272	22,179
	51CrSm [1]	0.78102–2.3208	6/6	4648	11,133
	81SaWoLa [15]	0.80974–1085.9	**65/64**	78,730	334,491
	96AlDyIlPo [27]	1.7684–4.9397	125/125	2422	31,532
	63TaSa [3]	1.8259–2.3595	8/8	3489	20,135
	17CeTaPuCh [102]	3.4770–1106.6	87/87	352,735	3,347,371
	12CaPu [46]	4.3201–35.499	15/15	194	1092
	03MaMaMaGa [99]	4.4699–5.0494	5/5	973	2094
	84CaLoFuCa [17]	8.0374–90.321	1142/1142	233,248	1,523,452
	05MuBr [36]	9.5512–66.301	297/297	9	316
	85HeLu [18]	14.693–31.462	118/118	2037	16,327
	01ScBeHuLi [34]	20.333–24.167	110/110	5116	47,838
	00MuFaCoBr [32]	61.176–106.68	13/13	1552	7582
	17UlBeGrBe [129]	975.13–1656.0	**2242/2228**	659,450	3,440,765
	13UlOnGrBe [48]	991.22–1457.0	**12,104/12,097**	67,056	933,505
	10TaChStGi [43]	1083.3–1103.4	72/72	432,090	9,750,057
	07ZeJoGrPa [37]	1088.2–1090.3	37/37	480,179	1,177,435
	08HeBaBa [38]	1325.4–1381.2	178/178	203,701	1,113,390
	92KuHeSuHe [22]	1325.7–1386.3	18/18	865,940	3,743,121
	88GuNaUl [21]	1331.4–1887.3	**114/112**	585,386	2,561,065
	11UlGrBeBo [44]	1566.3–1912.3	**6447/6434**	102,802	4,022,479
	98LaFlGu [29]	2214.3–2379.0	**1574/1571**	100,982	1,119,287
	14UlGrBeBe [49]	2423.9–3038.3	**2215/2208**	131,674	866,189
	96LaPiHiSa [128]	2458.8–2526.3	1261/1261	40,872	767,840
	77PiDrPaDa [11]	2463.5–2526.0	**2001/1999**	852,849	7,778,518
	77PiMo [12]	2463.5–2524.6	106/106	564,873	6,585,379
	12UlGrBeBo [45]	2620.1–2875.7	**5772/5769**	170,833	3,368,888
	93LaPiFlCa [25]	2667.6–2767.3	1229/1229	64,556	2,070,312
	10UlBeGrAl [42]	3598.7–4058.8	**345/344**	233,505	3,119,369
	92LaFrPiFl [24]	4018.2–4075.5	**760/758**	113,624	831,296
$^{33}S^{16}O_2$	78Lovas [13]	0.31998–1.9490	**62/59**	22,300	156,172
	00MuFaCoBr [32]	0.37941–2.2894	4/4	65,333	72,087
	64MoKiSaHi [5]	0.55492–1.0653	12/12	46,412	114,559
	97KlScBeWi [98]	17.960–31.608	**104/100**	21,805	1,673,831
	01ScBeHuLi [34]	21.706–24.142	9/9	1608	3234
	17BlFlLa [63]	447.09–637.71	**7413/7408**	107,026	1,477,578
	17FlBlLa [62]	1060.5–2514.6	**8043/8036**	122,086	1,350,160
$^{34}S^{16}O_2$	78Lovas [13]	0.10317–11.612	398/398	16,985	416,988
	79BeDrMa [14]	0.44057–0.59943	2/2	4183	4211
	64MoKiSaHi [5]	0.51402–1.1079	17/17	22,524	106,351
	64BaBe [4]	0.68541–1.3857	20/20	1686	12,522
	98BeTrKoKl [28]	1.0333–35.608	143/143	2092	163,035
	96AlDyIlPo [27]	1.9242–3.9520	45/45	2494	14,272
	85HeLu [18]	14.716–25.814	53/53	1673	7516
	01ScBeHuLi [34]	20.459–23.978	51/51	3943	17,558
	08LaFlNgSa [39]	428.31–1883.3	**13,846/13,843**	102,276	1,324,846
	10TaChStGi [43]	1083.4–1103.2	13/13	351,091	1,445,141
	17CeTaPuCh [102]	1083.4–1106.5	**12/11**	296,179	1,149,144
	07ZeJoGrPa [37]	1088.0–1089.7	5/5	489,446	616,843
	16UlBeGrBub [57]	1551.5–1888.5	3427/3427	170,656	1,224,744
	16UlBeGrBua [55]	2168.3–3003.7	**6672/6671**	168,056	1,699,335
	15UlGrBeKr [52]	2196.6–2839.8	**3837/3834**	185,992	1,168,166
	88GuNaUl [21]	2263.4–2297.9	16/16	979,562	2,170,522
	96LaPiHiSa [128]	2428.3–2503.1	1638/1638	168,035	1,723,885
	77PiDrPaDa [11]	2463.5–2497.3	101/101	1,873,001	8,678,387
	16UlBeGrFo [56]	3358.0–3465.7	792/792	201,965	1,121,438
$^{36}S^{16}O_2$	78Lovas [13]	0.282–1.286	31/31	–	–

[a] Tags denote experimental data sources used in this study. The column 'Range' indicates the range corresponding to validated wavenumber entries within the experimental linelist. 'A/V' is an ordered pair standing for the number of assigned transitions in the data source (A) and for the number of transitions validated in this paper (V), with **boldface** used when these differ. Two parameters (APAR and LAR), introduced in Eqs. (10)–(11), were calculated on the validated lines to characterize the quality of the data sources. The recalibration factors determined in this study are 0.999 999 816 for 93LaPiFlCa [25], 0.999 999 151 for 10TaChStGi [43], 0.999 999 263 for 17CeTaPuCh [102], 0.999 999 658 for 16UlBeGrBua [55], and 0.999 999 534 for 16UlBeGrBub [57]. The transitions utilized during this study from the sources 96LaPiHiSa [128], 98LaFlGu [29], 17BlFlLa [63], and 17FlBlLa [62] have been obtained from the authors of these publications.

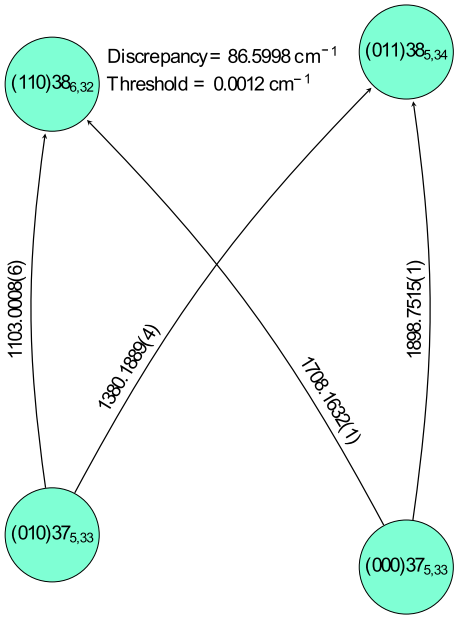

Fig. 1. The worst basic cycle of the $^{32}S^{16}O_2$ experimental spectroscopic network. Numbers on the arrows represent wavenumbers in cm^{-1}, with their initial uncertainties (see the text) given in parentheses. The transitions in this basic cycle were taken from 17CeTaPuCh [102], 08HeBaBa [38], and 11UlGrBeBo [44]. Levels are placed along a hypothetical vertical axis reflecting (qualitatively) their energy values. The "discrepancy" and the "threshold" were computed by means of Eqs. (5)–(6) and (10)–(16) of 17ToFuCs [120], respectively. After the execution of the ECART (Energy Conservation Analysis of Rovibronic Transitions) protocol, the line at 1103.0008 cm^{-1} was deleted.

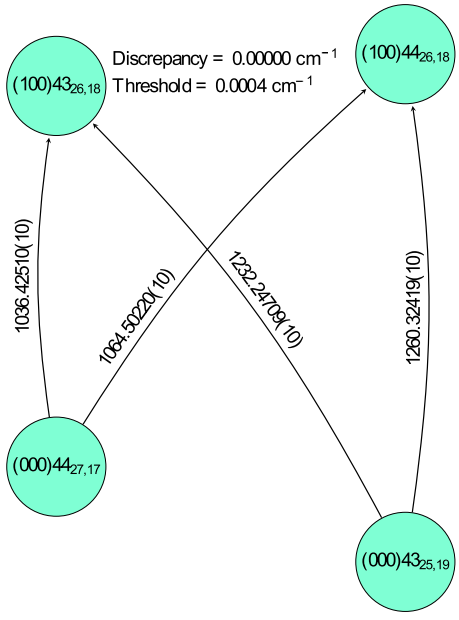

Fig. 2. A basic cycle with zero discrepancy in the $^{32}S^{16}O_2$ experimental spectroscopic network. Transitions were taken from 13UlOnGrBe [48]. Numbers on the arrows represent wavenumbers in cm^{-1}, with their initial uncertainties (see the text) given in parentheses. Levels are placed along a hypothetical vertical axis reflecting (qualitatively) their energy values. The discrepancy and the threshold were computed by means of Eqs. (5)–(6) and (10)–(16) of 17ToFuCs [120].

flect

$$|J' - J''| = \begin{cases} 1, & \text{if } (-1)^{(J'+K_c')} = (-1)^{(J''+K_c'')}, \\ 0, & \text{otherwise.} \end{cases} \quad (14)$$

It should be noted that selection rules were found to be violated only by 22, 3, and 8 lines, respectively, within the original experimental $^{32}S^{16}O_2$, $^{33}S^{16}O_2$, and $^{34}S^{16}O_2$ datasets. Of these, 10, 0, and 7 lines, respectively, could be reassigned (see below). The other lines were not considered further.

Due to measurements of the same transitions by several experiments, there are transitions in the compiled dataset that have the same labels – *i.e.*, they are *coincident*. The set of all transitions with a given label shall be referred to as a *coincidence class*. If conflicts occur among the transitions within a coincidence class, we are forced to select those lines that are in closest agreement with each other. Using a cut-off value of 0.04 cm^{-1} for the absolute wavenumber differences, only 3 transitions (92KuHeSuHe.3, 92KuHeSuHe.13, and 17CeTaPuCh.4) showed this type of deviance. However, these lines could all be reassigned at a later stage of our analysis.

Since certain papers report data from other studies, as well as their own, several coincidence classes contain *redundant* coincident transitions, characterized by identical wavenumbers and assignments. By means of an automated search, redundant lines were identified and sorted according to their year of publication in each coincidence class; only the earliest of each was kept in the final, collated experimental transition dataset.

MCB-based ECART analyses [120] were carried out for the $^{32}S^{16}O_2$, $^{33}S^{16}O_2$, and $^{34}S^{16}O_2$ experimental SNs. These analyses yielded 17, 1, and 1 lines for the $^{32}S^{16}O_2$, $^{33}S^{16}O_2$, and $^{34}S^{16}O_2$ datasets, respectively, that led to discrepancies larger than 0.01 cm^{-1} in the cycle basis. The worst basic cycle of the $^{32}S^{16}O_2$ linelist is shown in Fig. 1. It should also be noted that for the $S^{16}O_2$ isotopologues there are some basic cycles characterized with a discrepancy identically equal to zero (see Fig. 2). We believe this should not occur in a natural way and suggest that some of the actual data provided as measured may really correspond to the output of a conventional EH fit.

The length of a cycle is defined as the number of energy levels it contains. Most basic cycles in SNs are of length four, the minimal length allowed by symmetry. The fraction of total basic cycles with length greater than 4 with respect to the total number of basic cycles is a useful measure of the SN's topology. In the case of $S^{16}O_2$, many basic cycles with length greater than 4 come from 13UlOnGrBe [48], and this fraction (8.0, 2.9, and 3.5% for the $^{32}S^{16}O_2$, $^{33}S^{16}O_2$, and $^{34}S^{16}O_2$ networks, respectively) is considerably larger than that found in the case of water isotopologues [120]. Furthermore, there are plenty of spectroscopic bridges (originating mostly from 13UlOnGrBe [48], 08LaFlNgSa [39], and 16UlBeGrBua [55]) among the cycles, which may deteriorate the accuracy of some of the MARVEL energy levels.

Following the elimination of the outliers, as described above, a MARVEL analysis was executed, based on Eqs. (1)–(2), to determine the MARVEL energy levels of the three $S^{16}O_2$ isotopologues. In the experimental linelist supplied as Supplementary Material to this paper, the adjusted uncertainties consistent with the corresponding residuals are included.

Having the MARVEL energy levels determined from the experimental lines, it is mandatory to compare them to theoretically computed levels (see Section 5.4). While the MARVEL energy levels have a much lower uncertainty than their first-principles counterparts, they form an incomplete set and the occurrence of superfluous levels cannot be ruled out. Computed energy levels are orders of magnitude less accurate but they form a unique and complete set, a very important and highly useful property. In particular, we compared the MARVEL levels with levels computed on the semiempirically refined PES of 16UnTeYuHu [58] (*theoretical energy levels*), as these should in principle match nicely, within about 0.03 cm^{-1}, the MARVEL levels. Consequently, all experimental transitions incident to a rovibrational level whose energy value was located at a distance larger than 0.1 cm^{-1} from their theoreti-

Table 2
Statistical parameters[a] concerning the energy levels of the $^{32}S^{16}O_2$, $^{33}S^{16}O_2$, and $^{34}S^{16}O_2$ isotopologues.

	$^{32}S^{16}O_2$	$^{33}S^{16}O_2$	$^{34}S^{16}O_2$
NL	15,171	5854	10,899
NVL	15,130	5852	10,893
J_{max}	95	78	75
E_{max}	5302.452	3675.767	4239.943
ΔE_{max}	230.705	45.902	56.703
ΔE_{avg}	0.350	0.628	0.389
t_{max}	66	24	58
t_{avg}	5.2	5.2	5.7
s_{max}	18	5	13
s_{avg}	2.0	1.2	1.8
ϵ_{max}	0.00900	0.00059	0.00069
ϵ_{avg}	0.00011	0.00011	0.00013

[a] NL = the number of energy levels; NVL = the number of validated levels; E_{max} = the maximum energy value of the given dataset; ΔE_{max} and ΔE_{avg} are the maximum and average gap between two levels respectively; ϵ_{max} and ϵ_{avg} are the maximum and average uncertainties of the energy levels, respectively; t_{max} and t_{avg} are the maximum and average number of transitions incident to an energy level, respectively; s_{max} and s_{avg} are the maximum and average number of sources including an energy level, respectively. All energy-like quantities are given in cm^{-1}.

cal counterparts, were excluded from the database. In this manner, only 11(2), 0(0), and 6(1) lines had to be deleted(reassigned) in the $^{32}S^{16}O_2$, $^{33}S^{16}O_2$, and $^{34}S^{16}O_2$ SNs, respectively, which is very reassuring. That there are any such inconsistencies at all, however, likely stems from the handful of states we found necessary to reassign.

Next, for all available vibrational bands conventional EH fits were executed and the MARVEL energy levels were compared to their conventional EH counterparts. All MARVEL energy levels, which could not be matched with their conventional EH counterparts within 0.005 cm^{-1}, were excluded from the $S^{16}O_2$ databases, along with their transitions. Thus, 21(0), 13(0), and 17(0) transitions were deleted(reassigned) in the $^{32}S^{16}O_2$, $^{33}S^{16}O_2$, and $^{34}S^{16}O_2$ spectroscopic networks, respectively.

The final reassignments were made using partly the wavenumber-sorted experimental dataset, and partly a MARVEL linelist, ignoring transitions with $|K'_a - K''_a| > 2$. All non-validated lines were manually reassigned, applying a cut-off of 0.005 cm^{-1} in the absolute wavenumber difference and inspecting the similarity of the experimental and MARVEL-predicted transitions with respect to their assignment. Based on all this information, in the case of the $^{32}S^{16}O_2$ isotopologue, 18 lines were reassigned out of the 74 problematic ones. As to $^{33}S^{16}O_2$, 0 lines were reassigned out of 19, while 24 transitions of the 32 lines could be relabeled in the $^{34}S^{16}O_2$ experimental dataset.

5. Results: MARVEL energy levels and labels

5.1. MARVEL energy levels

The MARVEL energy levels of the $^{32}S^{16}O_2$, $^{33}S^{16}O_2$, and $^{34}S^{16}O_2$ molecules obtained in the final step of our analyses are characterized here. As shown in Table 2, the overwhelming majority of the MARVEL energy levels could be validated. Due to the large moments of inertia of the $S^{16}O_2$ species, the density of the rovibrational levels is quite large. For higher J values, larger gaps can be observed between the neighboring energy levels – indicating that several bands are missing from the dataset.

As to our confidence in the MARVEL energy levels, a six-grade quality ranking ($A^{\pm}$, $B^{\pm}$, $C^{\pm}$) is provided for each energy level. Our classification scheme is summarized in Table 3. The grades reflect the resistance and the number of transitions and data sources that incorporate the energy levels. As to the transitions, it is recommended that they should be assigned the lower of the two corresponding energy level grades. Energy levels with an A^+ grade are fully dependable; thus, they are especially important for future studies. They can safely be used, *e.g.*, for an empirical adjustment of the PES of SO_2. By contrast, C^- levels – which do not belong to any cycles, or have not been reproduced in multiple experiments – need further experimental validation. The dependability of rovibrational states with a C^+ grade is strongly influenced by the uncertainty of the bridges that connect them to the PCs. Levels with higher grades are more or less dependable, owing to their presence in cycles and to repeated measurements.

As an additional check, we formed the ratio of the corresponding $^{33}S^{16}O_2$ and $^{32}S^{16}O_2$ and the $^{34}S^{16}O_2$ and $^{32}S^{16}O_2$ energy levels and plotted the ratios as a function of rovibrational energy. The ratios change very smoothly. Thus, we conclude that the labels of the three $S^{16}O_2$ isotopologues are fully consistent.

5.2. Effective Hamiltonian fits

Having obtained reliable MARVEL energy levels for the rovibrational states of $^{32}S^{16}O_2$, $^{33}S^{16}O_2$, and $^{34}S^{16}O_2$, we next turn our attention to the labels of these states. SO_2 is by no means a "floppy" molecule, and so the vast majority of rovibrational state assignments presented in the literature are expected to be reliable. Nevertheless, there are a considerable number of MARVEL energy levels, extending up to quite large J values (J_{max} is 95, 78, and 75 for $^{32}S^{16}O_2$, $^{33}S^{16}O_2$, and $^{34}S^{16}O_2$, respectively), where the resonance interactions become pronounced even for a "semirigid" molecule. It is therefore certainly plausible that at least a few of the transitions and levels as reported in the experimental literature have been misassigned. Indeed, as discussed in Section 4, our analyses did uncover several such cases, leading to reassignments and deletions.

To assess the correctness of the published rovibrational assignments and the accuracy of our empirical levels, all the MARVEL energy levels were modeled using conventional EH models (see Section 2.2). Rovibrational parameters presented in the literature served as initial values for the conventional EH modeling. The results of the conventional EH fits are summarized in Table 4; the optimized parameters are given in the Supplementary Material. As can be seen from Table 4, the RMSDs obtained in this study are occasionally somewhat larger than those reported in the original papers. This can be explained, at least partly, by the fact that different lower-state energy levels have been used for the upper energy-level determinations in the literature as compared to this study. Furthermore, we did not intend to reproduce the literature EH results which sometimes assumed inclusion of coupling parameters of very high order. Generally, our aim has only been to run reasonable calculations capable of identifying problematic energy levels. Next, as the only example, details of the energy levels fitting for the lowest vibrational state (0 0 0) of $^{32}S^{16}O_2$ is discussed.

For the set of close to 2000 (0 0 0) energy levels of $^{32}S^{16}O_2$, J_{max} is 95 and the maximum K_a value is 35. Note that a number of transitions involving (0 0 0) energy levels up to $J = 110$ have been observed in 13UlOnGrBe [48] for the ν_1 band but these transitions could not be processed by MARVEL as they do not connect to the principal components of the measured SN. The initial set of rotational parameters for the (0 0 0) state was taken from 13UlOnGrBe [48], where the highest J and K_a values used were 110 and 35, respectively. 78 combination difference relations involving high K_a values, from 29 to 34, together with 149 accurate microwave transitions of 05MuBr [36] were used in 13UlOnGrBe

Table 3
The six-grade quality classification scheme[a] of the energy levels of $^{32}S^{16}O_2$, $^{33}S^{16}O_2$, and $^{34}S^{16}O_2$.

Grade	Resistance	$s \geq s^*$	$t \geq t^*$	$N(^{32}S^{16}O_2)$	$N(^{33}S^{16}O_2)$	$N(^{34}S^{16}O_2)$
A^+	Protected	Yes	Yes	3102	956	2451
A^-	Protected	Yes	No	1171	83	936
B^+	Protected	No	Yes	927	1240	900
B^-	Protected	No	No	6669	2790	4757
C^+	Semiprotected	–	–	48	0	68
C^-	Unprotected	–	–	3213	783	1781

[a] Resistance of an energy level is defined in Section 2. s and t are the number of sources and transitions, respectively, including the energy level. Using $s^* = 2$ and $t^* = 5$, based on s_{avg} and t_{avg} of Table 2, $N(S^{16}O_2)$ is the number of levels in the selected grade for the given $S^{16}O_2$ molecule. Grades provide information on the dependability of levels.

Table 4
Statistical information concerning the effective rotational Hamiltonian fits for all available vibrational bands of $^{32}S^{16}O_2$, $^{33}S^{16}O_2$, and $^{34}S^{16}O_2$.[a]

Species	Interacting vibrational bands	FRL	RMSD/cm^{-1}	MD/cm^{-1}	N_{out}	Source
$^{32}S^{16}O_2$	(0 0 0)	1997	0.000142	0.000879	41	13UlOnGrBe [48]
	(0 0 1), (1 0 0), (0 2 0)	3878	0.000150	0.001313	69	13UlOnGrBe [48]
	(0 0 2), (1 3 0)[b]	994	0.000334	0.002540	18	12UlGrBeBo [45]
	(0 0 3), (1 3 1)[b]	504	0.000276	0.001685	5	10UlBeGrAl [42]
	(0 1 0)	800	0.000309	0.002651	13	05MuBr [36]
	(0 1 1)	975	0.000309	0.003219	15	11UlGrBeBo [44]
	(0 1 2), (1 4 0)[b]	375	0.000355	0.002745	2	12UlGrBeBo [45]
	(0 1 3)	181	0.001034	0.003252	2	10UlBeGrAl [42]
	(0 3 0), (1 1 0)	1670	0.000598	0.004089	31	17UlBeGrBe [129], 11UlGrBeBo [44]
	(1 0 1), (0 2 1)	1337	0.000471	0.004701	32	96LaPiHiSa [128], 11UlGrBeBo [44]
	(1 1 1)	731	0.000340	0.004762	6	96LaPiHiSa [128]
	(2 0 0), (1 2 0)	1159	0.000206	0.001391	20	98LaFlGu [29], 11UlGrBeBo [44]
	(2 1 0)	439	0.000178	0.000865	7	12UlGrBeBo [45]
	(2 1 1)	90	0.001148	0.004440	2	10UlBeGrAl [42]
$^{33}S^{16}O_2$	(0 0 0)	1133	0.000288	0.002178	21	17FlBlLa [62]
	(0 0 1), (1 0 0)	2010	0.000309	0.002232	42	17FlBlLa [62]
	(0 1 0)	1097	0.000209	0.001211	25	17BlFlLa [63]
	(0 2 0)	813	0.000193	0.000958	17	17BlFlLa [63]
	(1 0 1)	799	0.000294	0.001168	12	17FlBlLa [62]
$^{34}S^{16}O_2$	(0 0 0)	1261	0.000209	0.001350	36	08LaFlNgSa [39]
	(0 0 1), (1 0 0), (0 2 0)	2736	0.000199	0.001649	52	08LaFlNgSa [39]
	(0 0 2), (1 3 0)[b]	820	0.000245	0.001152	8	15UlGrBeKr [52]
	(0 1 0)	1167	0.000179	0.001292	32	08LaFlNgSa [39]
	(0 1 1)	774	0.000209	0.001292	12	16UlBeGrBub [57]
	(0 3 0)[b], (1 1 0)	701	0.000390	0.002321	12	09LaFlNgSa [133], 08LaFlNgSa [39]
	(1 0 1), (0 2 1)	1311	0.000367	0.002106	25	96LaPiHiSa [128], 16UlBeGrBub [57]
	(1 1 1)	560	0.000341	0.001373	8	16UlBeGrBua [55]
	(2 0 0)	934	0.000378	0.004346	15	16UlBeGrBua [55]
	(2 1 0)	302	0.000259	0.001011	1	15UlGrBeKr [52]
	(3 0 0)	327	0.000294	0.000787	0	16UlBeGrFo [56]

[a] The second column lists the vibrational bands considered for each isotopologue. Where multiple vibrational bands are listed, their couplings were also taken into account. FRL = number of fitted rovibrational energy levels. In the columns "RMSD" and "MD" the root-mean-square and the maximum deviations of the fits are given, respectively. N_{out} = number of outlier MARVEL energy levels deviating more than 3× RMSD from their conventional EH counterparts. The column "Source" lists the sources where the initial values of the rovibrational parameters were taken from. The optimized conventional EH parameters can be found in the Supplementary Material to this paper.

[b] MARVEL energy levels are not available for these vibrational states.

[48] to refine the (0 0 0) spectroscopic constants. Although a RMSD of 1.4×10^{-4} cm^{-1} was obtained, by relaxing 19 parameters, for the whole dataset, after removing MARVEL energy levels having C^- grade and unsigned deviations larger than 3 × RMSD from their conventional EH counterparts (39 in total), the RMSD is reduced to 1.1×10^{-4} cm^{-1} with the maximum deviation of 0.0005 cm^{-1}. The set of parameters reported in 13UlOnGrBe [48] reproduces our set of 1997 MARVEL energy levels with an RMSD of 1.6×10^{-4} cm^{-1} compared to our 1.1×10^{-4} cm^{-1}.

The J-dependent rotational Hamiltonian fits also fully supported the labels for all (v, J) levels of $^{32}SO_2$ and $^{34}SO_2$, for which the experimental data are complete. The $^{32}S^{16}O_2$ dataset has a total of 3120 levels, distributed over 245 complete (v, J) pairs. The largest J value included is $J = 35$, corresponding to the ground vibrational state. The $^{34}S^{16}O_2$ dataset includes a total of 2893 levels, from 211 complete (v, J) classes. Here, the highest vibrational and rotational excitations correspond to $v = (3\ 0\ 0)$ and $J = 14$, respectively. The parameters of the J-dependent rotational Hamiltonians we arrived at in this study are summarized in the Supplementary Information.

5.3. Vibrational band origins (VBOs)

In Table 5 all the vibrational band origins (VBOs) revealed by experiments or provided by our conventional EH fits are given along with their uncertainties. Where the energy levels with $J = 0$ (a) cannot be observed experimentally, due to Eq. (12) (these are

Table 5
Vibrational band origins (VBOs) for $^{32}S^{16}O_2$, $^{33}S^{16}O_2$, and $^{34}S^{16}O_2$.[a]

P	v	$^{32}S^{16}O_2$				$^{33}S^{16}O_2$				$^{34}S^{16}O_2$			
		VBO/cm^{-1}	J_{min}	J_{max}	NRL	VBO/cm^{-1}	J_{min}	J_{max}	NRL	VBO/cm^{-1}	J_{min}	J_{max}	NRL
0	(0 0 0)	**0.000000(0)**	0	95	1997	**0.000000(0)**	0	78	1133	**0.000000(0)**	0	75	1261
1	(0 1 0)	**517.872470(3)**	0	63	800	**515.659373(200)**	0	72	1097	**513.539128(297)**	0	70	1167
2	(0 0 1)	1362.060210(16)	1	95	1654	1353.336097(37)	1	78	1120	1345.094701(24)	1	72	1136
	(0 2 0)	**1035.126485(2)**	0	54	369	**1030.697705(200)**	0	63	813	**1026.455335(200)**	0	60	794
	(1 0 0)	**1151.712963(3)**	0	88	1855	**1147.979601(200)**	0	68	890	1144.478649(27)	1	62	806
3	(0 1 1)	1875.797164(40)	1	67	975	–	–	–	–	1854.610532(29)	1	65	774
	(0 3 0)	**1551.729361(64)**	0	53	654	–	–	–	–	–	–	–	–
	(1 1 0)	1666.334250(73)	1	70	1016	–	–	–	–	1654.828981(44)	1	65	701
4	(0 0 2)	**2713.382105(3)**	0	75	994	–	–	–	–	2679.799845(27)	1	70	820
	(0 2 1)	2388.915251(68)	2	57	527	–	–	–	–	*2363.545841(62)*	2	44	303
	(1 0 1)	2499.870107(65)	1	61	810	2487.493888(40)	1	60	799	*2475.786361(36)*	1	74	1008
	(1 2 0)	2180.331224(28)	2	59	497	–	–	–	–	–	–	–	–
	(2 0 0)	**2295.808139(27)**	0	58	662	–	–	–	–	2281.469401(39)	1	64	934
5	(0 1 2)	*3222.972492(53)*	2	49	375	–	–	–	–	–	–	–	–
	(1 1 1)	3010.317368(40)	2	65	731	–	–	–	–	2982.119380(53)	1	65	560
	(2 1 0)	2807.188089(32)	2	43	439	–	–	–	–	2788.638623(49)	1	45	302
6	(0 0 3)	4054.001108(35)	1	58	504	–	–	–	–	–	–	–	–
	(3 0 0)	–	–	–	–	–	–	–	–	3410.975359(55)	1	49	327
7	(0 1 3)	4559.433952(234)	3	35	181	–	–	–	–	–	–	–	–
	(2 1 1)	4136.934473(353)	4	26	90	–	–	–	–	–	–	–	–

[a] v represents the normal-mode label of the given vibrational state. VBOs (with their uncertainties in parentheses) are sorted by the polyad number P defined as $P = 2v_1 + v_2 + 2v_3$. Data in boldface correspond to MARVEL energy levels, the other values are determined using conventional effective Hamiltonian (EH) fits. The conventional EH-based VBOs were taken from the same models as used in Table 4, except for the data in italic, which were obtained from refitting the current EH models with $^{vv'}F_0 = 0$ (see Eq. (5)). The columns J_{min} and J_{max} indicate the range of J values for the MARVEL energy levels connected to a particular vibrational state. NRL is the number of validated MARVEL energy levels associated with a particular vibrational state of the given $S^{16}O_2$ dataset.

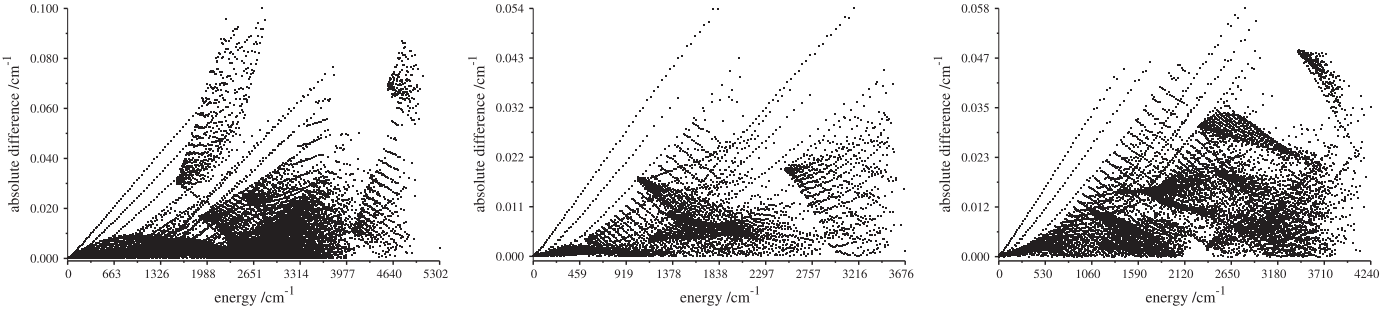

Fig. 3. Absolute differences between the MARVEL and ExoAmes [58] energy levels for $^{32}S^{16}O_2$ (left figure), the MARVEL and Ames [51] energy levels for $^{33}S^{16}O_2$ (middle figure), and the MARVEL and Ames [51] energy levels for $^{34}S^{16}O_2$ (right figure).

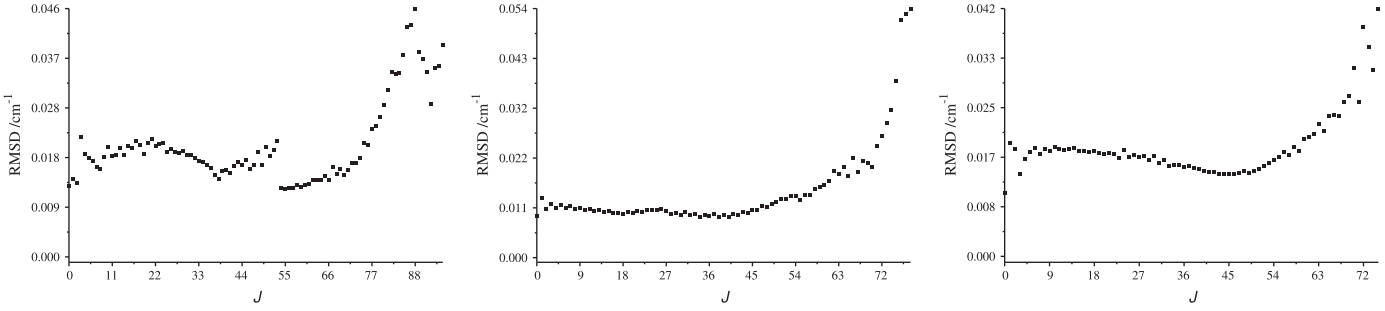

Fig. 4. Root-mean-square deviations (RMSD) at different J values for the MARVEL and ExoAmes [58] energy levels of $^{32}S^{16}O_2$ (left figure), the MARVEL and Ames [51] energy levels of $^{33}S^{16}O_2$ (middle figure), and the MARVEL and Ames [51] energy levels of $^{34}S^{16}O_2$ (right figure).

the vibrational bands with odd v_3) or (b) are not part of experimental transitions, the VBO parameters are taken from conventional EH models. It must be noted that only relatively few energy levels with $J = 0$ (19, 6, and 14 for $^{32}S^{16}O_2$, $^{33}S^{16}O_2$, and $^{34}S^{16}O_2$, respectively) are included in the experimental transitions; nevertheless, several rotational states were observed in cases where the VBOs are not derived from experiments. When comparing the VBOs of this study to those of 09UlBeAlHo [41], differences are found only in the fourth decimal place.

5.4. Comparison with theoretical energy levels

To highlight a possible application of the MARVEL energy levels of $^{32}S^{16}O_2$, $^{33}S^{16}O_2$, and $^{34}S^{16}O_2$, a comparison was performed with theoretically computed rovibrational states. For the $^{32}S^{16}O_2$ molecule, the "ExoAmes" list of levels [58] was applied, while the "Ames states" [51] were utilized for $^{33}S^{16}O_2$ and $^{34}S^{16}O_2$.

For the cleansed list of MARVEL energy levels and their theoretical counterparts, absolute differences and RMSDs at different J values are plotted in Figs. 3 and 4. In these charts patterns are

clearly visible, showing the systematic nature of the distortion of the theoretical levels. It can also be seen that all the deviations are less than 0.10, 0.05, and 0.06 cm^{-1} for the $^{32}S^{16}O_2$, $^{33}S^{16}O_2$, and $^{34}S^{16}O_2$ isotopologues, respectively, displaying the high quality of the PES adopted for the nuclear-motion computations. The total RMSDs are 0.019, 0.011, and 0.017 cm^{-1} for $^{32}S^{16}O_2$, $^{33}S^{16}O_2$, and $^{34}S^{16}O_2$, respectively.

6. Conclusions

The high-resolution rovibrational spectroscopy of the sulphur isotopologues of $S^{16}O_2$, on their ground $\tilde{X}^1A_1$ electronic state, is of substantial current interest, across a diverse range of scientific subdisciplines. In the astrophysical context, precise spectral signatures of the two most abundant species, $^{32}S^{16}O_2$ and $^{34}S^{16}O_2$, is most relevant, whereas in the astrobiology/paleogeology context, the rovibronic energy-level structures of $^{33}S^{16}O_2$ and $^{36}S^{16}O_2$ are also vitally important. In both contexts, precise knowledge of correctly assigned individual transitions/levels is needed. Thus, one of the principal goals of this study has been to make a significant step in this direction by collecting and analyzing all the available experimental high-resolution spectroscopic transition data.

Over the years, many experimental studies and theoretical computations have been performed for the $S^{16}O_2$ molecules. The high-resolution spectra of the $S^{16}O_2$ isotopologues is relatively straightforward to assign, owing to the large masses of the constituent atoms and the fairly rigid structure of the molecule. Nevertheless, the density of states is quite high, especially when the degree of vibrational and rotational excitation increases, increasing the likelihood of misassignments. Moreover, it was not until recently that theoretical PESs of sufficiently high quality were developed to provide useful rovibronic data. Using such PESs, rovibrational state computations can provide definitive guidance to experiment, *vis-à-vis* the determination of energy levels. However, quantum theory has difficulties to provide state labels of the desired $(\nu_1\nu_2\nu_3)J_{K_a,K_c}$ form even when such labels seem to be unambiguous based on conventional effective Hamiltonian (EH) fits.

To determine rovibrational energy levels and their assignments, sophisticated analysis methods are needed – forming a quite distinct class from both experimental spectral techniques and theoretical rovibrational state computations. MARVEL (Measured Active Rotational–Vibrational Energy Levels) is such a technique. As always, treating the incomplete set of accurate experimental transitions with MARVEL necessitates the use of the comparatively inaccurate but complete information available from first-principles computations.

In contrast to previous MARVEL-based studies devoted to the water molecule [130,134–137], in the present study EH fits were also executed to validate the MARVEL energy levels and their assignments and to discriminate less accurate data in the collated experimental database, which includes more than 87,000 transitions for the $S^{16}O_2$ isotopologues. The conventional EH fits contribute considerably to the reliability of the MARVEL energy levels obtained from the measured transition data. For the conventional EH calculations, root mean-square deviations from the MARVEL energy levels are on average less than 0.0005 cm^{-1}, using a conventional 43-parameter Hamiltonian operator with terms up to $\hat{J}^{12}$ (nevertheless, usually no more than 10–20 parameters for every vibrational state are fitted to reproduce hundreds of levels). The corresponding average uncertainties of MARVEL energy levels were nearly of the same degree, $\approx 10^{-4}$ cm^{-1}. We also utilized a *J*-dependent rotational Hamiltonian procedure, as a further means of data analysis.

By any criterion, the uncertainties are far smaller than the *J*-specific level spacing – supporting the validity of the final rovibrational labels obtained in this work. Overall, the experimental dataset was found to be remarkably consistent across the different sources, leading to a high degree of confidence in the levels and their assignments.

Acknowledgements

AGC is thankful to NKFIH for support (grant no. K119658). BP acknowledges support from NASA Astrobiology (NNX13AJ49G-EXO), together with both a research grant (CHE-1012662) and a CRIF MU instrumentation grant (CHE-0840493) from the National Science Foundation, as well as the Robert A. Welch Foundation (D-1523). The work of BP in Budapest was supported under invitation from the Hungarian Academy of Sciences Distinguished Guest Scientist program. OVN is grateful to the Russian Science Foundation for financial support (grant No. 17-12-01204). Dr. Xinchuan Huang is thanked for providing technical assistance in using the Ames data. The support of the COST action CM1405 (MOLIM: Molecules in Motion) is acknowledged. The authors are grateful to Prof. Oleg Ulenikov for fruitful discussions on some of the topics of this paper.

Supplementary material

Supplementary material associated with this article can be found, in the online version, at 10.1016/j.jqsrt.2018.01.006.

References

[1] Crable GF, Smith WV. The structure and dipole moment of SO_2 from microwave spectra. J Chem Phys 1951;19:502–3.
[2] Shelton RD, Nielsen AH, Fletcher WH. The infrared spectrum and molecular constants of sulfur dioxide. J Chem Phys 1953;21:2178–83.
[3] Takagi K, Saito S. Millimeter wave spectrum of SO_2. J Phys Soc Jpn 1963;18:1840.
[4] Bauer A, Bellet J. Spectre de rotation de SO_2 en ondes millimétriques. J de Phys 1964;25:805–8.
[5] Morino Y, Kikuchi Y, Saito S, Hirota E. Equilibrium structure and potential function of sulfur dioxide from the microwave spectrum in the excited vibrational state. J Mol Spectrosc 1964;13:95–118.
[6] Saito S. Microwave spectrum of sulfur dioxide in doubly excited vibrational states and determination of the γ constants. J Mol Spectrosc 1969;30:1–16.
[7] Hinkley ED, Calawa AR, Kelley PL, Clough SA. Tunable-laser spectroscopy of the ν_1 band of SO_2. J Appl Phys 1972;43:3222–4.
[8] Corice JRJ, Fox K, Tejwani GDT. Experimental and theoretical studies of the fundamental bands of sulfur dioxide. J Chem Phys 1973;58:265–70.
[9] Corice JRJ, Fox K, Tejwani GDT. $\nu_1+\nu_3$ combination band of $^{32}S^{16}O_2$. J Chem Phys 1973;59:672–5.
[10] Barbe A, Secroun C, Jouve P, Duterage B, Monnanteuil N, Bellet J, et al. High resolution spectra of $\nu_1+\nu_3$ and $(\nu_1+\nu_2+\nu_3)-\nu_2$ bands of SO_2. J Mol Spectrosc 1975;55:319–50.
[11] Pine AS, Dresselhaus G, Palm B, Davies RW, Clough SA. Analysis of the 4-μm $\nu_1+\nu_3$ combination band of SO_2. J Mol Spectrosc 1977;67:386–415.
[12] Pine AS, Moulton PF. Doppler-limited and atmospheric spectra of the 4-μm $\nu_1+\nu_3$ combination band of SO_2. J Mol Spectrosc 1977;64:15–30.
[13] Lovas FJ. Microwave spectral tables II. Triatomic molecules. J Phys Chem Ref Data 1978;7:1445–750.
[14] Bestmann G, Dreizler H, Mäder H. Investigation of Ti-relaxation with a microwave pulse spectrometer rotational lines of formaldehyde and sulfur dioxide. Z Naturforsch. A 1979;34:1330–3.
[15] Sattler JP, Worchesky TL, Lafferty WJ. Diode laser heterodyne spectroscopy on the ν_1 band of sulfur dioxide. J Mol Spectrosc 1981;88:364–71.
[16] Carter S, Mills IM, Murrell JN, Varandas AJC. Analytical potentials for triatomic molecules. IX. The prediction of anharmonic force constants from potential energy surfaces based on harmonic force fields and dissociation energies for SO_2 and O_3. Mol Phys 1982;45:1053–66.
[17] Carlotti M, Di Lonardo G, Fusina L, Carli B, Mencaraglia F. The submillimeter-wave spectrum and spectroscopic constants of SO_2 in the ground state. J Mol Spectrosc 1984;106:235–44.
[18] Helminger PA, De Lucia FC. The submillimeter wave spectrum of $^{32}S^{16}O_2$, $^{32}S^{16}O_2$ (ν_2), and $^{34}S^{16}O_2$. J Mol Spectrosc 1985;111:66–72.
[19] Lindenmayer J, Jones H, Typke V. Diode laser and IR–MW double resonance spectroscopy of the ν_1 band $^{32}S^{18}O_2$. J Mol Spectrosc 1985;110:357–63.
[20] Lindenmayer J, Jones H. Laser spectroscopy of sulfur dioxide: the ν_1 band of $^{32}S^{16}O^{18}O$ and the ν_3 band of $^{32}S^{18}O_2$. J Mol Spectrosc 1987;126:58–62.
[21] Guelachvili G, Naumenko OV, Ulenikov ON. On the analysis of some hyperweak absorption bands of SO_2 in the regions 1055–2000 and 2200–2550 cm. J Mol Spectrosc 1988;131:400–2.

[22] Kühnemann F, Heiner Y, Sumpf B, Herrmann K. Line broadening in the ν_3 band of SO_2: studied with diode laser spectroscopy. J Mol Spectrosc 1992;152:1–12.

[23] Kauppi E, Halonen L. A simple curvilinear internal coordinate model for vibrational energy levels of hydrogen sulfide and sulfur dioxide. J Chem Phys 1992;96:2933–41.

[24] Lafferty WJ, Fraser GT, Pine AS, Flaud J-M, Camy-Peyret C, Dana V, et al. The $3\nu_3$ band of $^{32}S^{16}O_2$: line positions and intensities. J Mol Spectrosc 1992;154:51–60.

[25] Lafferty WJ, Pine AS, Flaud J-M, Camy-Peyret C. The $2\nu_3$ band of $^{32}S^{16}O_2$: line positions and intensities. J Mol Spectrosc 1993;157:499–511.

[26] Cohen EA, Hillig KW, Pickett HM. The rotational spectra, hyperfine interactions, and ^{17}O magnetic shieldings of $^{17}O^{16}O^{16}O$, $^{16}O^{17}O^{16}O$, and $^{17}OS^{16}O$. J Mol Spectrosc 1995;352:273–82.

[27] Alekseev EA, Dyubko SF, Ilyushin VV, Podnos SV. The high-precision millimeter-wave spectrum of $^{32}SO_2$, $^{32}SO_2$ (ν_2), and $^{34}SO_2$. J Mol Spectrosc 1996;176:316–20.

[28] Belov SP, Tretyakov MY, Kozin IN, Klisch E, Winnewisser G, Lafferty WJ, et al. High frequency transitions in the rotational spectrum of SO_2. J Mol Spectrosc 1998;191:17–27.

[29] Lafferty WJ, Flaud J-M, Guelachvili G. Analysis of the $2\nu_1$ band system of SO_2. J Mol Spectrosc 1998;188:106–7.

[30] Ma G, Chen R, Guo H. Quantum calculations of highly excited vibrational spectrum of sulfur dioxide. I. Eigenenergies and assignments up to 15000 cm^{-1}. J Chem Phys 1999;110:8408–16.

[31] Ma G, Guo H. Quantum calculations of highly excited vibrational spectrum of sulfur dioxide. II. Normal to local mode transition and quantum stochasticity. J Chem Phys 1999;111:4032–40.

[32] Müller HSP, Farhoomand J, Cohen EA, Brupbacher-Gatehouse B, Schäfer M, Bauder A, et al. The rotational spectrum of SO_2 and the determination of the hyperfine constants and nuclear magnetic shielding tensors of $^{33}SO_2$ and $SO^{17}O$. J Mol Spectrosc 2000;201:1–8.

[33] Zúñiga J, Bastida A, Requena A. Optimal generalized internal vibrational coordinates and potential energy surface for the ground electronic state of SO_2. J Chem Phys 2001;115:139–48.

[34] Schilke P, Benford DJ, Hunter TR, Lis DC, Phillips TG. A line survey of Orion-KL from 607 to 725 GHz. Astrophys J, Suppl Ser 2001;132:281.

[35] Varandas AJC, Rodrigues SPJ. Realistic double many-body expansion potential energy surface for $SO_2(\tilde{X}^1A_1)$ from a multiproperty fit to accurate ab initio energies and vibrational levels. Spectrochim Acta A Mol Biomol Spectrosc 2002;58:629–47.

[36] Müller HSP, Brünken S. Accurate rotational spectroscopy of sulfur dioxide, SO_2, in its ground vibrational and first excited bending states, $\nu_2 = 0, 1$, up to 2 THz. J Mol Spectrosc 2005;232:213–22.

[37] Zéninari V, Joly L, Grouiez B, Parvitte B, Barbe A. Study of SO_2 line parameters with a quantum cascade laser spectrometer around 1090 cm^{-1}: comparison with calculations of the ν_1 and $\nu_1 + \nu_2 - \nu_2$ bands of $^{32}SO_2$ and the ν_1 band of $^{34}SO_2$. J Quant Spectrosc Radiat Transfer 2007;105(2):312–25.

[38] Henningsen J, Barbe A, De Backer-Barilly M-R. Revised molecular parameters for $^{32}SO_2$ and $^{34}SO_2$ from high resolution study of the infrared spectrum in the 7–8 μm wavelength region. J Quant Spectrosc Radiat Transfer 2008;109:2491–510.

[39] Lafferty WJ, Flaud J-M, Sams RL, Ngom EHA. High resolution analysis of the rotational levels of the (000), (010), (100), (001), (020), (110), and (011) vibrational states of $^{34}S^{16}O_2$. J Mol Spectrosc 2008;252:72–6.

[40] Ulenikov ON, Bekhtereva ES, Horneman V-M, Alanko S, Gromova OV. High resolution study of the $3\nu_1$ band of SO_2. J Mol Spectrosc 2009;255:111–21.

[41] Ulenikov ON, Bekhtereva ES, Alanko S, Horneman V-M, Gromova OV, Leroy C. On the high resolution spectroscopy and intramolecular potential function of SO_2. J Mol Spectrosc 2009;257:137–56.

[42] Ulenikov ON, Bekhtereva ES, Gromova OV, Alanko S, Horneman V-M, Leroy C. Analysis of highly excited 'hot' bands in the SO_2 molecule: $\nu_2 + 3\nu_3 - \nu_2$ and $2\nu_1 + \nu_2 + \nu_3 - \nu_2$. Mol Phys 2010;108:1253–61.

[43] Tasinato N, Charmet AP, Stoppa P, Giorgianni S, Buffa G. Spectroscopic measurements of SO_2 line parameters in the 9.2 μm atmospheric region and theoretical determination of self-broadening coefficients. J Chem Phys 2010;132:044315.

[44] Ulenikov ON, Gromova OV, Bekhtereva ES, Bolotova IB, Leroy C, Horneman V-M, et al. High resolution study of the $\nu_1 + 2\nu_2 - \nu_2$ and $2\nu_2 + \nu_3 - \nu_2$ "hot" bands and ro-vibrational re-analysis of the $\nu_1 + \nu_2/\nu_2 + \nu_3/3\nu_2$ polyad of the $^{32}SO_2$ molecule. J Quant Spectrosc Radiat Transfer 2011;112:486–512.

[45] Ulenikov ON, Gromova OV, Bekhtereva ES, Bolotova IB, Konov IA, Horneman V-M, et al. High resolution analysis of the SO_2 spectrum in the 2600–region: $2\nu_3$, $\nu_2 + 2\nu_3 - \nu_2$ and $2\nu_1 + \nu_2$ bands. J Quant Spectrosc Radiat Transfer 2012;113:500–17.

[46] Cazzoli G, Puzzarini C. N_2-, O_2-, H_2-, and He-broadening of SO_2 rotational lines in the mm-/submm-wave and THz frequency regions: the J and K_a dependence. J Quant Spectrosc Radiat Transfer 2012;113:1051–7.

[47] Dong-Lan W, An-Dong X, Xiao-Guang Y, Hui-Jun W. The analytical potential energy function of flue gas $SO_2(\tilde{X}^1A_1)$. Chin Phys B 2012;21:043103.

[48] Ulenikov ON, Onopenko GA, Gromova OV, Bekhtereva ES, Horneman V-M. Re-analysis of the (100), (001), and (020) rotational structure of SO_2 on the basis of high resolution FTIR spectra. J Quant Spectrosc Radiat Transfer 2013;130:220–32.

[49] Ulenikov ON, Gromova OV, Bekhtereva ES, Belova AS, Bauerecker S, Maul C, et al. High resolution analysis of the (111) vibrational state of SO_2. J Quant Spectrosc Radiat Transfer 2014;144:1–10.

[50] Huang X, Schwenke DW, Lee TJ. Highly accurate potential energy surface, dipole moment surface, rovibrational energy levels, and infrared line list for $^{32}S^{16}O_2$ up to 8000 cm^{-1}. J Chem Phys 2014;140:114311.

[51] Huang X, Schwenke DW, Lee TJ. Empirical infrared line lists for five SO_2 isotopologues: $^{32/33/34/36}S^{16}O_2$ and $^{32}S^{18}O_2$. J Mol Spectrosc 2015;311:19–24.

[52] Ulenikov ON, Gromova OV, Bekhtereva ES, Krivchikova YV, Sklyarova EA, Buttersack T, et al. High resolution FTIR study of $^{34}S^{16}O_2$: the bands $2\nu_3$, $2\nu_1 + \nu_2$ and $2\nu_1 + \nu_2 - \nu_2$. J Mol Spectrosc 2015;318:26–33.

[53] Kumar P, Ellis J, Poirier B. Rovibrational bound states of SO_2 isotopologues. I: total angular momentum J=0–10. Chem Phys 2015;450–451:59–73.

[54] Kumar P, Poirier B. Rovibrational bound states of SO_2 isotopologues. II: total angular momentum J=11–20. Chem Phys 2015;461:34–46.

[55] Ulenikov ON, Bekhtereva ES, Gromova OV, Buttersack T, Sydow C, Bauerecker S. High resolution FTIR study of $^{34}S^{16}O_2$: the bands $2\nu_1$, $\nu_1 + \nu_3$, $\nu_1 + \nu_2 + \nu_3 - \nu_2$ and $\nu_1 + \nu_2 + \nu_3$. J Quant Spectrosc Radiat Transfer 2016;169:49–57.

[56] Ulenikov ON, Gromova OV, Bekhtereva ES, Fomchenko AL, Sydow C, Bauerecker S. First high resolution analysis of the $3\nu_1$ band of $^{34}S^{16}O_2$. J Mol Spectrosc 2016;319:50–4.

[57] Ulenikov ON, Bekhtereva ES, Gromova OV, Buttersack T, Sydow C, Bauerecker S. High resolution FTIR study of $^{34}S^{16}O_2$: re-analysis of the bands $\nu_1 + \nu_2$, $\nu_2 + \nu_3$, and first analysis of the hot band $2\nu_2 + \nu_3 - \nu_2$. J Mol Spectrosc 2016;319:17–25.

[58] Underwood DS, Tennyson J, Yurchenko SN, Huang X, Schwenke DW, Lee TJ, et al. Exomol molecular line lists–XIV. the rotation–vibration spectrum of hot SO_2. Mon Not Royal Astron Soc 2016;459:3890–9.

[59] Ulenikov ON, Bekhtereva ES, Gromova OV, Zamotaeva VA, Sklyarova EA, Sydow C, et al. First high resolution analysis of the $2\nu_1$, $2\nu_3$, and $\nu_1 + \nu_3$ bands of $S^{18}O_2$. J Quant Spectrosc Radiat Transfer 2016;185:12–21.

[60] Ulenikov ON, Bekhtereva ES, Krivchikova YV, Zamotaeva VA, Buttersack T, Sydow C, et al. Study of the high resolution spectrum of $^{32}S^{16}O^{18}O$: the ν_1 and ν_3 bands. J Quant Spectrosc Radiat Transfer 2016;168:29–39.

[61] Ulenikov ON, Bekhtereva ES, Gromova OV, Zamotaeva VA, Kuznetsov SI, Sydow C, et al. First high resolution analysis of the $\nu_1 + \nu_2$ and $\nu_2 + \nu_3$ bands of $S^{18}O_2$. J Quant Spectrosc Radiat Transfer 2016;179:187–97.

[62] Flaud J-M, Blake T, Lafferty W. First high-resolution analysis of the ν_1, ν_3, and $\nu_1 + \nu_3$ bands of sulphur dioxide $^{33}S^{16}O_2$. Mol Phys 2017;115:447–53.

[63] Blake TA, Flaud J-M, Lafferty WJ. First analysis of the rotationally-resolved ν_2 and $2\nu_2 - \nu_2$ bands of sulfur dioxide, $^{33}S^{16}O_2$. J Mol Spectrosc 2017;333:19–22.

[64] Warneck P, Marmo FF, Sullivan JO. Ultraviolet absorption of SO_2: dissociation energies of SO_2 and so. J Chem Phys 1964;40(4):1132–6.

[65] Brand JCD, Humphrey DR, Douglas AE, Zanon I. The resonance fluorescence spectrum of sulfur dioxide. Can J Phys 1973;51:530–6.

[66] Brand JCD, Chiu PH, Hoy AR, Bist HD. Sulfur dioxide: rotational constants and asymmetric structure of the $\tilde{C}^1B_2$ state. J Mol Spectrosc 1976;60:43–56.

[67] Hoy AR, Brand JCD. Asymmetric structure and force field of the $^1B_2(^1A)$ state of sulphur dioxide. Mol Phys 1978;36:1409–20.

[68] Freeman DE, Yoshino K, Esmond JR, Parkinson WH. High resolution absorption cross section measurements of SO_2 at 213 K in the wavelength region 172–240 nm. Planet Space Sci 1984;32:1125–34.

[69] Yamanouchi K, Yamada H, Tsuchiya S. Vibrational level structure of highly excited SO_2 in the electronic ground state as studied by stimulated emission pumping spectroscopy. J Chem Phys 1988;88:4664–70.

[70] Yamanouchi K, Takeuchi S, Tsuchiya S. Vibrational level structure of highly excited SO_2 in the electronic ground state. II. Vibrational assignment by dispersed fluorescence and stimulated emission pumping spectroscopy. J Chem Phys 1990;92:4044–54.

[71] Kamiya K, Matsui H. Theoretical studies on the potential energy surfaces of SO_2: electronic states for photodissociation from the $\tilde{C}^1B_2$ state. Bull Chem Soc Japan 1991;64:2792–801.

[72] Yamanouchi K, Okunishi M, Endo Y, Tsuchiya S. Laser induced fluorescence spectroscopy of the $\tilde{C}^1B_2$–$\tilde{X}^1A_1$ band of jet-cooled SO_2: rotational and vibrational analyses in the 235-210 nm region. J Mol Struct 1995;352–353:541–59.

[73] Katagiri H, Sako T, Hishikawa A, Yazaki T, Onda K, Yamanouchi K, et al. Experimental and theoretical exploration of photodissociation of SO_2 via the $\tilde{C}^1B_2$ state: identification of the dissociation pathway. J Mol Struct 1997;413–414:589–614.

[74] Okazaki A, Ebata T, Mikami N. Degenerate four-wave mixing and photofragment yield spectroscopic study of jet-cooled SO_2 in the $\tilde{C}^1B_2$ state: internal conversion followed by dissociation in the $\tilde{X}$ state. J Chem Phys 1997;107:8752–8.

[75] Sako T, Hishikawa A, Yamanouchi K. Vibrational propensity in the predissociation rate of SO_2 ($\tilde{C}^1B_2$) by two types of nodal patterns in vibrational wavefunctions. Chem Phys Lett 1998;294:571–8.

[76] Stark G, Smith PL, Rufus J, Thorne AP, Pickering JC, Cox G. High resolution photoabsorption cross section measurements of SO_2 at 295 K between 198 and 220 nm. J Geophys Res Planets 1999;104:16.

[77] Xie D, Ma G, Guo H. Quantum calculations of highly excited vibrational spectrum of sulfur dioxide. III. Emission spectra from the $\tilde{C}^1B_2$ state. J Chem Phys 1999;111:7782–8.

[78] Nachtigall P, Hrušák J, Bludskỳ O, Iwata S. Investigation of the potential energy surfaces for the ground $\tilde{X}^1A_1$ and excited $\tilde{C}^1B_2$ electronic states of SO_2. Chem Phys Lett 1999;303:441–6.

[79] Bludskỳ O, Nachtigall P, Hrušák J, Jensen P. The calculation of the vibrational states of SO in the $\tilde{C}^1B_2$ electronic state up to the $SO(^3\Sigma^-)$+$O(^3P)$ dissociation limit. Chem Phys Lett 2000;318:607–13.

[80] Li A, Suo B, Wen Z, Wang Y. Potential energy surfaces for low-lying electronic states of SO_2. Sci China B: Chem 2006;49:289–95.
[81] Lyons JR. Mass-independent fractionation of sulfur isotopes by isotope-selective photodissociation of SO_2. Geophys Res Lett 2007;34:L22811.
[82] Ran H, Xie D, Guo H. Theoretical studies of $\tilde{C}^1B_2$ absorption spectra of SO_2 isotopologues. Chem Phys Lett 2007;439:280–3.
[83] Lyons JR. Photolysis of long-lived predissociative molecules as a source of mass-independent isotope fractionation: the example of SO_2. Adv Quantum Chem 2008;55:57–74.
[84] Tokue I, Nanbu S. Theoretical studies of absorption cross sections for the $\tilde{C}^1B_2$–$\tilde{X}^1A_1$ system of sulfur dioxide and isotope effects. J Chem Phys 2010;132:024301.
[85] Ono S, Whitehill AR, Lyons JR. Contribution of isotopologue self-shielding to sulfur mass-independent fractionation during sulfur dioxide photolysis. J Geophys Res Atmos 2013;118:2444–54.
[86] Xie C, Hu X, Zhou L, Xie D, Guo H. Ab initio determination of potential energy surfaces for the first two uv absorption bands of SO_2. J Chem Phys 2013;139:014305.
[87] Lévêque C, Komainda A, Taïeb R, Köppel H. Ab initio quantum study of the photodynamics and absorption spectrum for the coupled 1^1A_2 and 1^1B_1 states of SO_2. J Chem Phys 2013;138:044320.
[88] Endo Y, Danielache SO, Ueno Y, Hattori S, Johnson MS, Yoshida N, et al. Photoabsorption cross-section measurements of ^{32}S, ^{33}S, ^{34}S, and ^{36}S sulfur dioxide from 190 to 220 nm. J Geophys Res Atmos 2015;120:2546–57.
[89] Park GB, Womack CC, Whitehill AR, Jiang J, Ono S, Field RW. Millimeter-wave optical double resonance schemes for rapid assignment of perturbed spectra, with applications to the $\tilde{C}^1B_2$ state of SO_2. J Chem Phys 2015;142:144201.
[90] Kłos J, Alexander MH, Kumar P, Poirier B, Jiang B, Guo H. New ab initio adiabatic potential energy surfaces and bound state calculations for the singlet ground $\tilde{X}^1A_1$ and excited $\tilde{C}^1B_2$ ($2^1A'$) states of SO_2. J Chem Phys 2016;144:174301.
[91] Park GB, Jiang J, Field RW. The origin of unequal bond lengths in the $\tilde{C}^1B_2$ state of SO_2: signatures of high-lying potential energy surface crossings in the low-lying vibrational structure. J Chem Phys 2016;144:144313.
[92] Jiang J, Park GB, Field RW. The rotation-vibration structure of the SO_2 $\tilde{C}^1B_2$ state explained by a new internal coordinate force field. J Chem Phys 2016;144:144312.
[93] Park GB, Jiang J, Saladrigas CA, Field RW. Observation of b_2 symmetry vibrational levels of the SO_2 $\tilde{C}^1B_2$ state: vibrational level staggering, coriolis interactions, and rotation-vibration constants. J Chem Phys 2016;144:144311.
[94] Kumar P, Jiang B, Guo H, Klos J, Alexander MH, Poirier B. Photoabsorption assignments for the $\tilde{C}^1B_2 \leftarrow \tilde{X}^1A_1$ vibronic transitions of SO_2, using new ab initio potential energy and transition dipole surfaces. J Phys Chem A 2017;121:1012–21.
[95] Jiang B, Kumar P, Kłos J, Alexander MH, Poirier B, Guo H. First-principles C band absorption spectra of SO_2 and its isotopologues. J Chem Phys 2017;146:154305.
[96] Xie C, Jiang B, Kłos J, Kumar P, Alexander MH, Poirier B, et al. Final state resolved quantum predissociation dynamics of SO_2 ($\tilde{C}^1B_2$) and its isotopologues via a crossing with a singlet repulsive state. J. Phys. Chem. A 2017;121:4930–8.
[97] Snyder LE, Hollis JM, Ulich BL, Lovas FJ, Johnson DR, Buhl D. Radio detection of interstellar sulfur dioxide. Astrophys J 1975;198:L81–4.
[98] Klisch E, Schilke P, Belov SP, Winnewisser G. $^{33}SO_2$: interstellar identification and laboratory measurements. J Mol Spectrosc 1997;186:314–18.
[99] Martin S, Mauersberger R, Martin-Pintado J, Garcia-Burillo S, Henkel C. First detections of extragalactic SO_2, NS, and NO. Astron Astrophys 2003;411:L465–8.
[100] Martín S, Martín-Pintado J, Mauersberger R, Henkel C, García-Burillo S. Sulfur chemistry and isotopic ratios in the starburst galaxy NGC 253. Astrophys J 2005;620:210.
[101] Visscher C, Lodders K, Fegley Jr B. Atmospheric chemistry in giant planets, brown dwarfs, and low-mass dwarf stars II. Sulfur and phosphorus. Astrophys J 2006;648:1181.
[102] Ceselin G, Tasinato N, Puzzarini C, Charmet AP, Stoppa P, Giorgianni S. CO_2-, He-, and H_2-broadening coefficients of SO_2 for ν_1 band and ground state transitions for astrophysical applications. J Quant Spectrosc Radiat Transfer 2017;203:367–76.
[103] Farquhar J, Bao H, Thiemens M. Atmospheric influence of earth's earliest sulfur cycle. Science 2000;289:756–8.
[104] Farquhar J, Savarino J, Airieau S, Thiemens MH. Observation of wavelength-sensitive mass-independent sulfur isotope effects during SO_2 photolysis: implications for the early atmosphere. J Geophys Res Planets 2001;106:32829–39.
[105] Farquhar J, Wing BA. Multiple surface isotopes and the evolution of the atmosphere. Earth Planet Sci Lett 2003;213:1–13.
[106] Pavlov AA, Kasting JF. Mass-independent fractionation of sulfur isotopes in archean sediments: strong evidence for an anoxic archean atmosphere. Astrobiology 2002;2:27–41.
[107] Halevy I, Johnston DT, Schrag DP. Explaining the structure of the archean mass-independent sulfur isotope record. Science 2010;329:204–7.
[108] Domagal-Goldman S.D., Poirier B., Wing B.. Summary report from workshop on mass-independent fractionation of sulfur isotopes: carriers and sources. 2012.
[109] Whitehill AR, Xie C, Hu X, Xie D, Guo H, Ono S. Vibronic origin of sulfur mass-independent isotope effect in photoexcitation of SO_2 and the implications to the early earth's atmosphere. Proc Natl Acad Sci USA 2013;110:17697–702.
[110] Polyansky OL, Császár AG, Shirin SV, Zobov NF, Barletta P, Tennyson J, et al. High-accuracy *ab initio* rotation-vibration transitions for water. Science 2003;299:539–42.
[111] Zak EJ, Tennyson J. Ro-vibronic transition intensities for triatomic molecules from the exact kinetic energy operator; electronic spectrum for the $\tilde{C}\ ^1B_2 \leftarrow \tilde{X}\ ^1A_1$ transition in SO_2. J Chem Phys 2017;147:094305.
[112] Rothman L, Gordon I, Babikov Y, Barbe A, Chris Benner D, Bernath P, et al. The HITRAN2012 molecular spectroscopic database. J Quant Spectrosc Radiat Transfer 2013;130:4–50.
[113] Kroto HW. Molecular rotation spectra. Dover, New York; 1992.
[114] Furtenbacher T, Császár AG, Tennyson J. MARVEL: measured active rotational–vibrational energy levels. J Mol Spectrosc 2007;245:115–25.
[115] Császár AG, Czakó G, Furtenbacher T, Mátyus E. An active database approach to complete spectra of small molecules. Ann Rep Comp Chem 2007;3:155–76.
[116] Furtenbacher T, Császár AG. On employing $H_2^{16}O$, $H_2^{17}O$, $H_2^{18}O$, and $D_2^{16}O$ lines as frequency standards in the 15 – 170 cm^{-1} window. J Quant Spectrosc Radiat Transfer 2008;109:1234–51.
[117] Császár AG, Furtenbacher T. Spectroscopic networks. J Mol Spectrosc 2011;266:99–103.
[118] Furtenbacher T, Császár AG. MARVEL: measured active rotational–vibrational energy levels. II. Algorithmic improvements. J Quant Spectrosc Radiat Transfer 2012;113:929–35.
[119] Császár AG, Furtenbacher T, Árendás P. Small molecules – big data. J Phys Chem A 2016;120:8949–69.
[120] Tóbiás R, Furtenbacher T, Császár AG. Cycle bases to the rescue. J Quant Spectrosc Radiat Transfer 2017;203:557–64.
[121] Gross J, Yellen J, Zhang P. Handbook of graph theory. Discrete Mathematics and Its Applications. 2nd ed. CRC Press; 2013.
[122] Watson JKG. Robust weighting in least-squares fits. J Mol Spectrosc 2003;219:326–8.
[123] Watson JKG. Determination of centrifugal distortion coefficients of asymmetric-top molecules. J Chem Phys 1967;46:1935–48.
[124] Watson JKG. Determination of centrifugal distortion coefficients of asymmetric-top molecules. II. Dreizler, Drendl, and Rudolph's results. J Chem Phys 1968;48:181–5.
[125] Watson JKG. Determination of centrifugal distortion coefficients of asymmetric-top molecules. III. Sextic coefficients. J Chem Phys 1968;48(10):4517–24.
[126] Watson JKG. Aspects of quartic and sextic centrifugal effects on rotational energy levels. Vibrational Spectra and Structure, 6. Amsterdam: Elsevier Scientific Publishing; 1977.
[127] Ulenikov O, Onopenko G, Koivusaari M, Alanko S, Anttila R. High resolution Fourier-transform spectrum of H_2S in the 3300–4080 cm^{-1} region. J Mol Spectrosc 1996;176:236–50.
[128] Lafferty WJ, Pine AS, Hilpert G, Sams RL, Flaud J-M. The $\nu_1+\nu_3$ and $2\nu_1+\nu_3$ band systems of SO_2: Line positions and intensities. J Mol Spectrosc 1996;176:280–6.
[129] Ulenikov ON, Bekhtereva ES, Gromova OV, Berezkin KB, Horneman V-M, Sydow C, et al. First high resolution analysis of the $3\nu_2$ and $3\nu_2-\nu_2$ bands of $^{32}S^{16}O_2$. J Quant Spectrosc Radiat Transfer 2017;202:1–5.
[130] Tennyson J, Bernath PF, Brown LR, Campargue A, Császár AG, Daumont L, et al. IUPAC critical evaluation of the rotational–vibrational spectra of water vapor. Part III: energy levels and transition wavenumbers for $H_2^{16}O$. J Quant Spectrosc Rad Transfer 2013;117:29–58.
[131] Jacquinet-Husson N, Armante R, Scott NA, Chedin A, Crepeau L, Boutammine C, et al. The 2015 edition of the GEISA spectroscopic database. J Mol Spectrosc 2016;327:31–72.
[132] Gordon I, Rothman L, Hill C, Kochanov RV, Tan Y, Bernath P, et al. The HITRAN2016 molecular spectroscopic database. J Quant Spectrosc Radiat Transfer 2017;203:3–69.
[133] Lafferty WJ, Flaud J-M, Sams RL, Ngom EHA. $^{34}S^{16}O_2$ high resolution analysis of the (030), (101), (111), (002), and (201) vibrational states; determination of equilibrium rotational constants for sulfur dioxide and anharmonic vibrational constants. J Mol Spectrosc 2009;253:51–4.
[134] Tennyson J, Bernath PF, Brown LR, Campargue A, Carleer MR, Császár AG, et al. Critical evaluation of the rotational–vibrational spectra of water vapor. Part I. Energy levels and transition wavenumbers for $H_2^{17}O$ and $H_2^{18}O$. J Quant Spectrosc Radiat Transfer 2009;110:573–96.
[135] Tennyson J, Bernath PF, Brown LR, Campargue A, Carleer MR, Császár AG, et al. Critical evaluation of the rotational–vibrational spectra of water vapor. Part II. Energy levels and transition wavenumbers for $HD^{16}O$, $HD^{17}O$, and $HD^{18}O$. J Quant Spectrosc Radiat Transfer 2010;110:2160–84.
[136] Tennyson J, Bernath PF, Brown LR, Campargue A, Császár AG, Daumont L, et al. IUPAC critical evaluation of the rotational–vibrational spectra of water vapor. Part IV. Energy levels and transition wavenumbers for $D_2^{16}O$, $D_2^{17}O$, and $D_2^{18}O$. J Quant Spectrosc Radiat Transfer 2014;142:93–108.
[137] Tennyson J, Bernath PF, Brown LR, Campargue A, Császár AG, Daumont L, et al. A database of water transitions from experiment and theory. Pure Appl Chem 2014;86:71–83. (IUPAC Technical Report)